Carbohydrate Polymers 114 (2014) 407–415

Contents lists available at ScienceDirect

Carbohydrate Polymers

journal homepage: www.elsevier.com/locate/carbpol

# Hyaluronic acid-coated solid lipid nanoparticles for targeted delivery of vorinostat to CD44 overexpressing cancer cells

Tuan Hiep Tran[a], Ju Yeon Choi[a], Thiruganesh Ramasamy[a], Duy Hieu Truong[a], Chien Ngoc Nguyen[b], Han-Gon Choi[c], Chul Soon Yong[a,**], Jong Oh Kim[a,*]

[a] College of Pharmacy, Yeungnam University, 214-1, Dae-Dong, Gyeongsan 712-749, South Korea
[b] National Institute of Pharmaceutical Technology, Hanoi University of Pharmacy, 13-15 Le Thanh Tong, Hoan Kiem, Ha Noi, Viet Nam
[c] College of Pharmacy, Hanyang University, 55, Hanyangdaehak-ro, Sangnok-gu, Ansan 426-791, South Korea

ARTICLE INFO

*Article history:*
Received 18 June 2014
Received in revised form 4 August 2014
Accepted 5 August 2014
Available online 23 August 2014

*Keywords:*
Vorinostat
Solid lipid nanoparticles
Hyaluronic acid
Chemotherapy
Targeting

ABSTRACT

Hyaluronic acid (HA)-decorated solid lipid nanoparticles (SLNs) were developed for tumor-targeted delivery of vorinostat (VRS), a histone deacetylase inhibitor. HA, a naturally occurring polysaccharide, which specifically binds to the CD44 receptor, was coated on a cationic lipid core through electrostatic interaction. After the optimization process, HA-coated VRS-loaded SLNs (HA-VRS-SLNs) were spherical, core-shell nanoparticles, with small size (~100 nm), negative charge (~−9 mV), and narrow size distribution. In vitro release profile of HA-VRS-SLNs showed a typical bi-phasic pattern. In addition, the intracellular uptake of HA-VRS-SLNs was significantly enhanced in CD44 overexpressing cells, A549 and SCC-7 cells, but reduced when HA-VRS-SLNs were incubated with SCC-7 cells pretreated with HA or MCF-7 cells with low over-expressed CD44. Of particular importance, HA-VRS-SLNs were more cytotoxic than the free drug and VRS-SLNs in A549 and SCC-7 cells. In addition, HA shell provided longer blood circulation and reduced VRS clearance rate in rats, resulting in enhanced higher plasma concentration and bioavailability. These results clearly indicated the potential of the HA-functionalized lipid nanoparticle as a nano-sized drug formulation for chemotherapy.



## 1. Introduction

Vorinostat (VRS), a histone deacetylase inhibitor, has been approved by the FDA for treatment of cutaneous T-cell lymphoma (CTCL) (Cai et al., 2010; Choo, Ho & Lin, 2008). In clinical trials, it was used for a variety of hematopoietic and solid tumor indications (Bolden, Peart & Johnstone, 2006; Kelly et al., 2005). It can effectively induce cell cycle arrest, cell differentiation, and apoptosis (Marks & Breslow, 2007). Despite showing such chemotherapeutic promise, the clinical application of VRS has been restricted due to its poor aqueous solubility and low membrane permeability, belonging to class IV of the Biopharmaceutics Classification System (BCS) (Mohamed et al., 2012). In addition, VRS exhibited a short half-life of 40 min following intravenous (IV) administration. To overcome these problems, VRS has been incorporated into micelle nanocarriers (Mohamed et al., 2012), inclusion cyclodextrins (Cai et al., 2010), and silicon microstructures (Strobl, Nikkhah & Agah, 2010), however, the efficiency of therapy is still a major question.

Solid lipid nanoparticles (SLNs) are a suitable candidate for delivery of hydrophobic and hydrophilic anti-cancer drugs. Owing to their lipid core, SLNs are expected to show high drug loading capacity, overcome multidrug resistance (MDR), modulate release kinetics, improve the blood circulation time, and increase the overall therapeutic efficacy of anti-cancer drugs (Bhushan et al., 2012; Lee, Lim & Kim, 2007; Luan et al., 2014). In addition, surface modification of SLNs with targeting moiety enables these SLNs to increase their selectivity for cellular binding and internalization (Venishetty, Komuravelli, Kuncha, Sistla & Diwan, 2013). In particular, the frequent overexpression of the hyaluronic acid (HA) receptors CD44 and CD168 (RHAMM) on many types of tumors opens new avenues for targeting by the naturally-occurring high-molecular weight HA (Rivkin, Cohen, Koffler, Melikhov, Peer & Margalit, 2010; Sun, Benjaminsen, Almdal & Andresen, 2012).

Therefore, in this study, we developed HA-coated VRS-loaded SLNs (HA-VRS-SLNs) for tumor-targeted delivery. We hypothesize that this system will demonstrate the combined advantages of high drug loading capacity by using lipid core, long blood circulation resulting from the hydrophilic surface and improved delivery

* Corresponding author. Tel.: +82 53 810 2813; fax: +82 53 810 4654.
** Corresponding author. Tel.: +82 53 810 2812; fax: +82 53 810 4654.
*E-mail addresses:* csyong@yu.ac.kr (C.S. Yong), jongohkim@yu.ac.kr (J.O. Kim).

http://dx.doi.org/10.1016/j.carbpol.2014.08.026
0144-8617/

by selective target of HA. To validate that, we investigated at the molecular, cellular, and whole animal levels of organization. The optimized HA-VRS-SLNs were evaluated in terms of physicochemical, thermal analyses, and ultrastructure characterization. The targeting efficacy of the HA-VRS-SLNs to tumor cells was estimated by intracellular uptake through confocal fluorescence image as well as flow-cytometric analysis in different cancer cell lines; the activity of VRS of HA-VRS-SLNs was then confirmed via cytotoxicity study. VRS plasma concentration, retention time and $AUC_{0-\infty}$ in blood circulation were compared among free drug, VRS-SLNs, and HA-VRS-SLNs for the *in vivo* study.

## 2. Materials and methods

### 2.1. Materials

VRS was purchased from LC Laboratories (MA, USA). Compritol 888 ATO (Compritol) (powder state; melting point, 70 °C) was obtained from Gattefosse (Cedex, France). 3-(4,5-Dimethylthiazol-2-yl)-2,5-diphenyl-tetrazolium bromide (MTT) and didecyldimethyl ammonium bromide (DDAB) were purchased from Sigma (St. Louis, MO, USA). Soybean lecithin was purchased from Junsei Co. Ltd (Tokyo, Japan). Hyaluronic acid (3 kDa) was supplied by B&K Technology Group Co. Ltd. (China). NBD-PC was supplied by Avanti Polar Lipids, Inc., and Lyso TrackerRed was purchased from Thermo Fisher Scientific Inc. The squamous cell carcinoma (SCC-7), human breast adenocarcinoma (MCF-7), human lung adenocarcinoma epithelial (A549) cells were originally obtained from the Korean Cell Line Bank (Seoul, South Korea). All cell lines were cultured in RPMI 1640 containing 10% fetal bovine serum (FBS), 100 U/mL penicillin G sodium, and 100 μg/mL streptomycin sulfate (complete 1640 medium) and incubated at 37 °C in 5% $CO_2$ atmosphere. All the cells threats such as fungi, bacteria, and mycoplasma were checked before carrying out experiments. All other chemicals were of reagent grade and were used without further purification.

### 2.2. Preparation of HA-VRS-SLNs

HA-VRS-SLNs were prepared by the hot homogenization method using an emulsification-sonication technique (Tran et al., 2014a). Based on a preliminary analysis of potential lipids and surfactants (data not shown), Compritol 888 ATO, DDAB, lecithin, and Tween 80 were selected for preparation of SLNs. Briefly, the lipid phase was prepared by melting Compritol 888 ATO, DDAB, lecithin, and VRS at 10 °C above the lipid melting point to obtain a clear transparent solution. The aqueous phase was prepared by dissolving Tween 80 in distilled water and heating to the final temperature of the lipid phase. Next, hot aqueous phase was gently added dropwise into the lipid phase with constant stirring at 13,500 rpm in an Ultra Turrax® T-25 homogenizer (IKA®-Werke, Staufen, Germany) for 3 min. The resulting coarse emulsion was immediately sonicated using a high-intensity probe sonicator (Vibracell VCX130; Sonics, USA) at 80% amplitude for 10 min. The resulting suspension was then cooled in an ice bath. For preparation of HA-VRS-SLNs, 1 mL of VRS-SLNs dispersion was slowly added under gentle stirring to a HA solution. The various concentrations of HA were investigated in order to obtain the optimum formulation.

Trehalose (5%, w/v) was used as a cryoprotectant in the freeze-drying process. The resulting nanoparticle dispersions were poured into glass bottles and pre-frozen at −80 °C for 24 h; later, the samples were freeze-dried using a lyophilizer (FDA5518, IlShin, South Korea) at a temperature of −25 °C for 24 h. The lyophilized powders were collected for further experiments.

### 2.3. Characterization of HA-VRS-SLNs

#### 2.3.1. Measurement of particle size and zeta potential

Particle sizes of VRS-SLNs and HA-VRS-SLNs were analyzed by the dynamic light scattering (DLS) technique using a Zetasizer Nano–Z (Malvern Instruments, Worcestershire, UK) at a fixed scattering angle of 90° and a temperature of 25 °C. Prior to the measurement, colloidal dispersions were adequately diluted with distilled water. DLS results are presented as *z*-average diameter, polydispersity index (PDI), and ζ-potential. The data were determined using the Nano DTS software (version 6.34) provided by the manufacturers. All measurements were performed in triplicate.

#### 2.3.2. Morphological analysis

The VRS-SLNs and HA-VRS-SLNs were deposited onto the surface of a copper grid (mesh size of 300) coated with carbon. Using 2% phosphotungstic acid (w/v), negative staining was performed on the samples, followed by air-drying for 15 min. The stained grids were subsequently probed using transmission electron microscopy (TEM) (Hitachi H-7100, Japan) to visualize the morphology of nanoparticles.

#### 2.3.3. Physical characterization

Differential scanning calorimetry (DSC) analysis were performed using a differential scanning calorimeter DSC-Q200 (TA Instruments, New Castle, DE, USA) for lipid, drug and optimized formulation. Briefly, 2–3 mg lyophilized sample was loaded in an aluminum pan and then heated over the temperature range of 40–200 °C with the heating rate of 10 °C/min under nitrogen gas flow of 50 mL/min. An empty pan was used as a reference. The XRD patterns of the above mentioned samples were obtained using an X-ray diffractometer (X'Pert PRO MPD diffractometer, Almelo, The Netherlands) using Cu $K_\alpha$ radiation under voltage of 40 kV and current of 30 mA with a scan step size of 0.02.

### 2.4. Drug entrapment efficiency and drug loading capacity

The drug entrapment efficiency (EE) and drug loading capacity (LC) of VRS-SLNs and HA-VRS-SLNs were determined by measuring the amount of free drug in the dispersion medium. Ultrafiltration was performed on the VRS-SLNs and HA-VRS-SLNs using centrifugal 10-kDa molecular weight cut-off devices (Amicon Ultra, Millipore, USA). 2 mL of formulations was dispensed onto the top compartment of the devices, followed by centrifuging at 5000 rpm for 10 min. The filtrate was collected and diluted with acetonitrile at a ratio of 1:1. The amount of free VRS in the aqueous phase was determined using high-performance liquid chromatography (HPLC). Formic acid (0.1%)/acetonitrile (70/30) was used as a mobile phase at a flow rate of 1.0 mL/min. VRS was detected at 241 nm. The drug entrapment efficiency and drug loading capacity were calculated using the following equations (Tran et al., 2014a).

$$EE(\%) = (W_{\text{initial drug}} - W_{\text{unbound drug}})/W_{\text{initial drug}} \times 100$$

$$LC(\%) = (W_{\text{initial drug}} - W_{\text{unbound drug}})/W_{\text{lipid}} \times 100$$

where EE is the entrapment efficiency; LC is the drug loading capacity; W is the weight (in mg)

### 2.5. In vitro release studies

The in vitro release behavior of VRS-SLNs and HA-VRS-SLNs was determined in dissolution medium composed of phosphate buffered saline (pH 7.4) using a dialysis method (Luan et al., 2014; Tran et al., 2014b). 1 mL of formulation was applied in the dialysis bag with a 3500 Da cut-off (Spectra/Por®, CA, USA). The dialysis

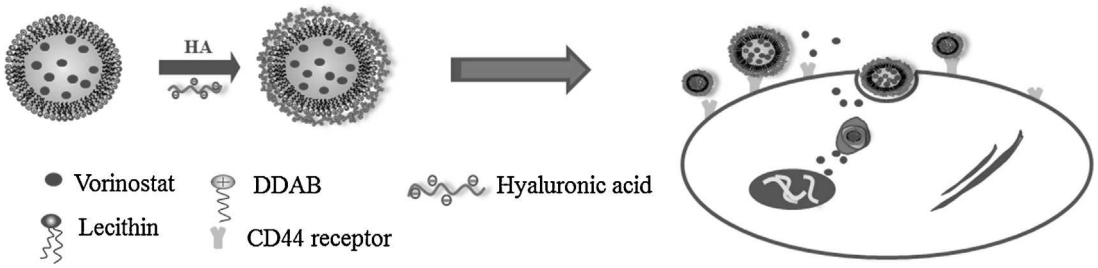


**Fig. 1.** Diagram illustrating the preparation process for HA-VRS-SLNs.

bag was soaked in a Falcon tube containing 40 mL of dissolution medium. The tube was capped and placed on a shaking water bath (HST–205 SW, Hanbaek ST Co., Korea) at 37 °C with a shaking speed of 100 rpm. The VRS released into the medium at each time point was taken and determined using the HPLC system described above.

### 2.6. In vitro cytotoxicity studies and cellular uptake

#### 2.6.1. Flow cytometric analysis

Cells ($2 \times 10^5$ cells/mL) were seeded in each well of a 6-well plate and incubated for 24 h using RPMI 1640 as media. 200 μL of RPMI 1640 (with or without HA at concentration 1 mg/mL) was added for 2 h, and the medium was then discarded and the cells were washed twice with phosphate buffered saline (PBS, pH 7.4). The cells were then treated with NBD-PC-loaded HA-SLNs at a concentration of 1 μg/mL in a humidified incubator with 5% $CO_2$ atmosphere at 37 °C. After incubation for 30 min, the medium was removed and washed twice with 2 mL of PBS. Cells were then harvested using 0.25% (w/v) trypsin solution then dispersed in 1.5 mL of PBS for flow cytometric measurements using a FACS Calibur flow cytometer (BD Biosciences, San Jose, CA, USA).

#### 2.6.2. Qualitative cellular uptake study by fluorescent microscopy

Cellular uptake of VRS-SLNs and HA-VRS-SLNs was evaluated by confocal microscopy in SCC-7 and MCF-7 cells. In detail, $2 \times 10^5$ cells per well were cultured in 12-well plates containing an antiseptic glass coverslip at the bottom of each well and incubated to grow overnight. Cells were continuously treated with 1 μg/mL NBD-PC loaded VRS-SLNs and HA-VRS-SLNs for 30 min, followed by continuous treatment with Lyso-Tracker Red and incubation for 10 min. Cells were then fixed with 4% paraformaldehyde for 15 min after washing three times with PBS. The glass coverslip with the cells was then taken out of the well and placed on a regular glass slide in the presence of mounting agent. Confocal analysis was performed on a Leica TCS SP2 Confocal Microscope (Leica Co., Wetzlar, Germany).

#### 2.6.3. In vitro cytotoxicity studies

Cell-killing activity of VRS-SLNs and HA-VRS-SLNs was measured using the MTT assay with some adjustments (Tran et al., 2014b). 100 μL of cell suspension with $5 \times 10^3$ cells/mL were cultured into wells of 96-well test plates and incubated for 24 h at 37 °C in 5% $CO_2$. A concentration range of blank SLNs, blank HA-SLNs, free VRS, VRS-SLNs, and HA-VRS-SLNs were added to each well-plate, followed by incubation for 24 h. The medium with sample was removed and then washed twice with phosphate-buffered saline. 100 μL MTT solution (1.25 mg/mL MTT in supplemented RPMI medium) was added to the cultures, followed by incubation for 4 h at 37 °C. The obtained formazan crystals were dissolved in 100 μL DMSO. Subsequently, an incubation of 15 min under light protection and at room temperature was performed. The absorbance was measured at 570 nm using a microplate reader (Multiskan EX, Thermo Scientific, Waltham, MA, USA). Cell viability was calculated using the following formula:

$$\text{Cell viability}(\%) = \frac{OD_{570}(\text{sample}) - OD_{570}(\text{blank})}{OD_{570}(\text{control}) - OD_{570}(\text{blank})} \times 100$$

The half-maximal inhibitory concentration ($IC_{50}$) of each group was calculated using GraphPad Prism 5 software.

### 2.7. Pharmacokinetics study

#### 2.7.1. Intravenous administration of VRS formulations to rats

Male Sprague-Dawley rats weighing 250 ± 10 g were divided into three groups of four rats. The animals were quarantined in an animal house maintained at 25 ± 2 °C and 50–60% RH, and fasted for 12 h prior to the experiments. The protocols for the animal studies were approved by the Institutional Animal Ethical Committee, Yeungnam University, South Korea.

Three groups of rats received free VRS, VRS-SLNs, and HA-VRS-SLNs by intravenous administration (Tran et al., 2014b). For IV injection of free VRS, VRS was dissolved in PEG 400 and administered at a dose of 10 mg/kg. In case of HA-VRS-SLNs, the lyophilized powder was dissolved in physiological saline (0.9% NaCl) at VRS concentration of 3 mg/mL, accordingly. The pH of solution is 6.4 before injection. Blood samples (300 μL) were collected from the right femoral artery at pre-determined times (0.25, 0.5, 1, 2, 3, 4, 6, 8, 12 and 24 h) after administration of these formulations. The samples were collected in heparin-containing tubes (100 IU/mL) and then immediately centrifuged (Eppendorf, Hauppauge, NY, USA) at 14,000 rpm for 10 min. The plasma supernatant was collected and stored at −20 °C until further analysis.

#### 2.7.2. Plasma sample processing

For extraction of VRS and for precipitation of unwanted protein, 150 μL of plasma was mixed with 150 μL of acetonitrile for 15 min. The samples were then centrifuged at 13,000 rpm for 10 min and 20 μL of the supernatant was injected into the HPLC system for VRS analysis, as described above.

#### 2.7.3. Analysis of pharmacokinetic data

The pharmacokinetic profiles of free VRS, VRS-SLNs, and HA-VRS-SLNs were calculated using the Win-NonLin pharmacokinetic software (v4.0, Pharsight Software, Mountain View, CA, USA). The pharmacokinetic data measured consisting of the area under curves of the plasma drug concentration-time from time zero to infinity ($AUC_{0-\infty}$), the half-life of elimination ($t_{1/2}$), and the mean residence time (MRT) were obtained by summation of the central and tissue compartments. Analysis of variance (ANOVA) was performed to investigate differences between the experimental treatments. A $p$-value < 0.05 was considered statistically significant in all cases, and all data were expressed as mean ± standard deviation.

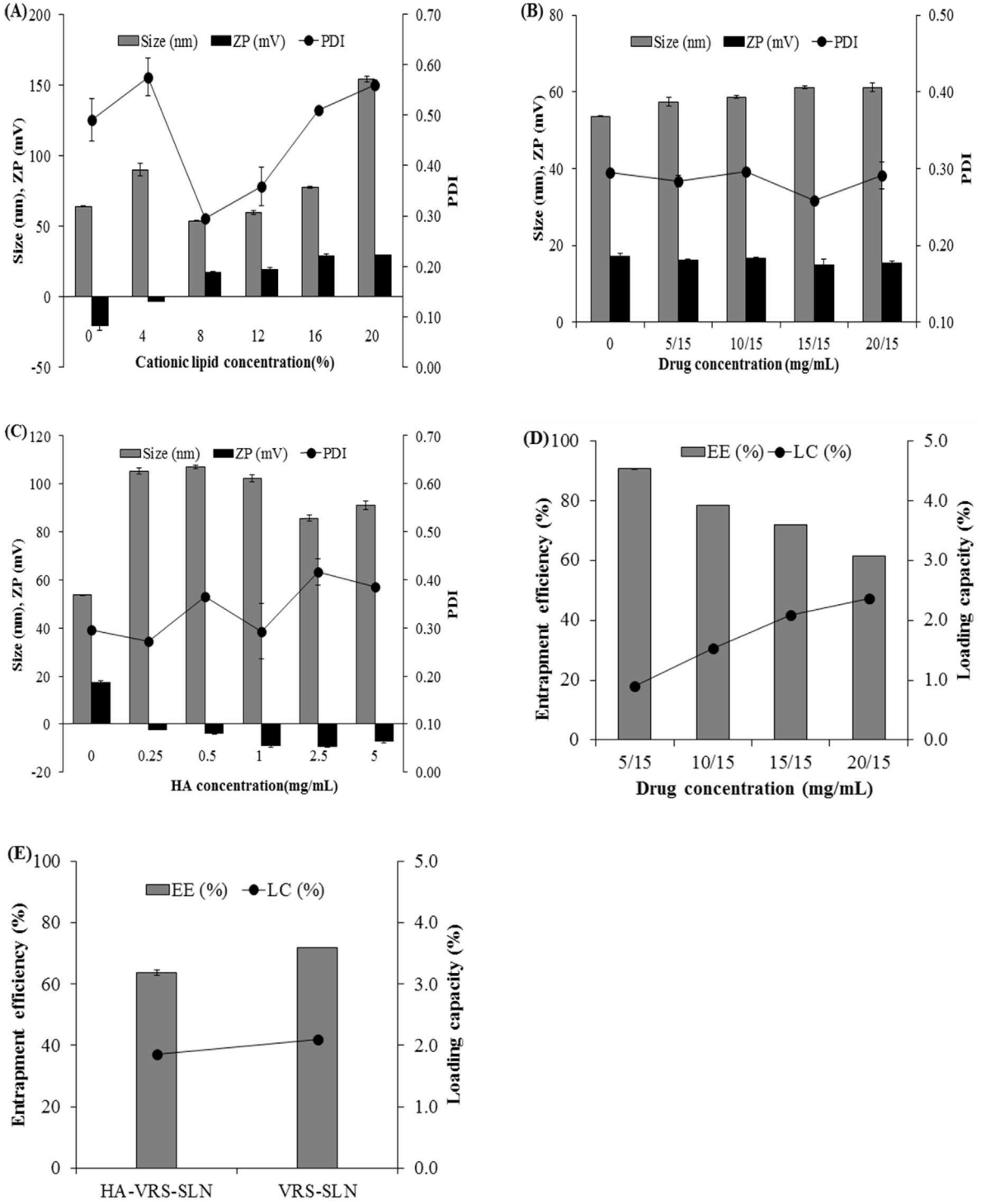


**Fig. 2.** Effect of (A) Cationic lipid concentration, (B) Drug concentration, (C) HA concentration on formulation parameters: particle size, polydispersity index (PDI), zeta potential (ZP). Effect of (D) drug concentration and (E) HA coating on drug entrapment efficiency and loading capacity. Data are expressed as the mean ± S.D. ($n = 3$).

## 3. Results and discussion

### 3.1. Preparation of HA-VRS-SLNs

HA-VRS-SLNs were developed using a cationic solid lipid core and then shedding by anionic polymer, HA (Fig. 1), in order to selectively and preferentially interact with tumor cell surface for effective cancer treatment. As shown in Fig. 1, the core of cationic SLNs was prepared using Compritol as a solid lipid element. Lecithin, DDAB, and Tween 80 were used as helper lipid, cationic lipid, and surfactant, respectively. Fig. 2**A** shows that SLNs were fabricated in particles with average sizes in the range of 50 and 150 nm, and polydispersity index (PDI) of 0.2 and 0.6. Cationic lipid concentration had significant effects on the system, especially PDI and surface charge. Zeta potential measurements determined the surface charge of all particles in aqueous medium in the range

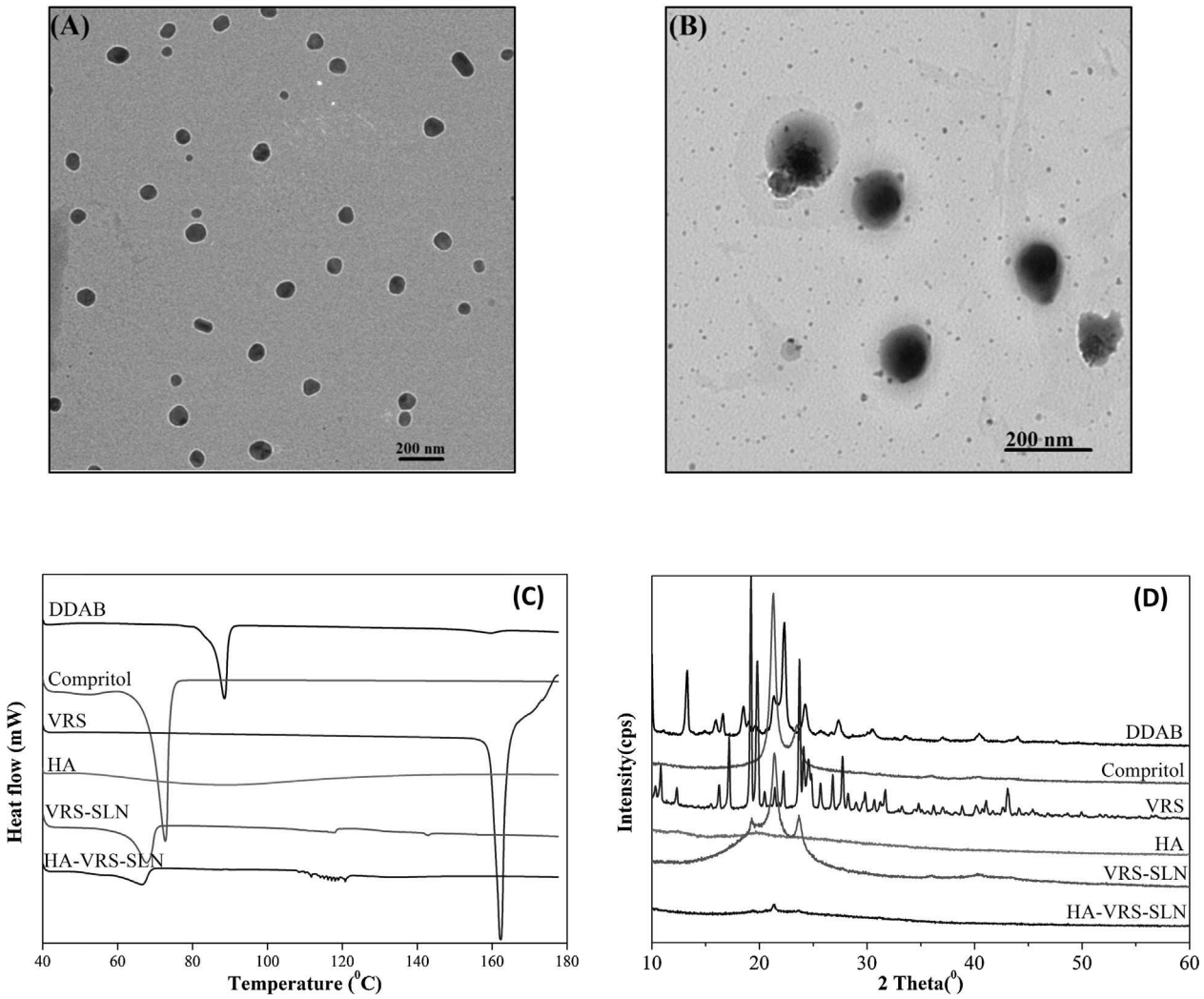


**Fig. 3.** TEM images of (A) VRS-SLNs and (B) HA-VRS-SLNs. (C) Differential scanning calorimetric thermograms and (D) X-ray diffraction patterns of DDAB, Compritol, free VRS, VRS-SLNs, and HA-VRS-SLNs.

between −20.6 and +29.3 mV. In the presence of 8% DDAB as a cationic lipid, VRS was incorporated into SLNs in order to find the optimal formulation. VRS-loaded SLNs were maintained in terms of size, PDI, and surface charge (Fig. 2**B**). The resulting cationic SLNs were covered with HA via electrostatic interaction. The outer layer of HA dramatically increased particle size and converted the surface charge to a negative charge. When the HA concentration increased, the surface charge also increased, but beyond 1 mg/mL the charge remained constant (Fig. 2**C**). The drug entrapment efficiency and loading capacity demonstrated compatible encapsulation of hydrophobic compound into the lipid core. Upon increase of drug amount, the drug loading capacity was augmented whereas the drug entrapment efficiency was reduced (Fig. 2**D**). This phenomenon is consisted with previous reports (Martins, Sarmento, Nunes, Lúcio, Reis & Ferreira, 2013; Raza, Singh, Singal, Wadhwa & Katare, 2013).

Finally, the formulation, which is composed of 40 mg DDAB as a cationic lipid, 460 mg Compritol, 100 mg Lecithin, 500 mg Tween 80, 15 mg VRS and then coating by 1 mg/mL HA solution was selected for further studies with small size (102.3 ± 1.6 nm), narrow distribution (0.293 ± 0.057), negative charge (−9.0 ± 0.7 mV) and high drug loading (1.86 ± 0.01%). The particles were stored and checked over at least three months, indicating long-term physical stability (data not shown).

### 3.2. Physical characterization

TEM photomicrographs of the optimized VRS-SLNs and HA-VRS-SLNs are shown in Fig. 3**A** and **3B**. Morphology of both formulations is spherical in shape and well supported by DLS characterization results. Nanoparticles appeared in the range of 60 nm and 110 nm, respectively. In particular, the structure of HA-VRS-SLNs was clearly observed with a black core and transparent shell indicating the HA layer.

DSC and X-ray diffraction were performed for VRS, lipid, HA, VRS-SLNs and HA-VRS-SLNs for characterization of the drug–lipid interactions and the crystallinity of drug before and after formulation in lipid matrices. As shown in Fig. 3**C**, DSC thermogram of bulk compritol, DDAB showed sharp melting peaks at 73 °C and 88 °C, respectively, whereas VRS exhibited a melting peak at 163 °C, corresponding to their natural crystal forms. In contrast, VRS-SLNs and HA-VRS-SLNs did not show the endothermic peak for the VRS around 163 °C. This finding indicates that VRS was in amorphous state or incorporated inside the lipid core (Ramasamy et al., 2014). In addition, sharp peaks were observed for VRS at 2θ-scattered angles of 16.3, 17.2, 19.2, 19.8, 22.2, and 23.7, corresponding to the crystalline nature of the drug, whereas the crystalline state of Compritol was still presented at 2θ-scattered angles of 21.3 and 23.5 (Fig. 3**D**). The intensity of VRS and Compritol peaks was decreased

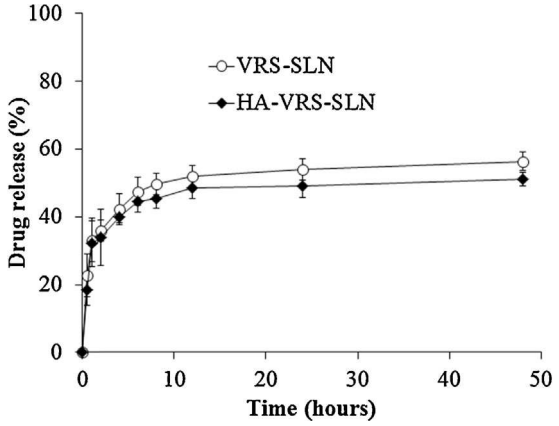


**Fig. 4.** *In vitro* drug release of VRS from VRS-SLNs (○) and HA-VRS-SLNs (♦) in PBS buffer (pH 7.4, 0.14 M NaCl) at 37 °C. Data are expressed as mean ± S.D. ($n = 3$).

in VRS-SLNs and HA-VRS-SLNs. Less ordered crystal lattices of lipid suggested the successful drug-lipid interaction. In addition, less ordered lipids prevent expulsion of the drug from the particles. Thus, Compritol provides more space for accommodation of drug molecules and limits drug expulsion (Peer, Karp, Hong, Farokhzad, Margalit & Langer, 2007).

### 3.3. In vitro drug release

In vitro release profiles of VRS from VRS-SLNs and HA-VRS-SLNs formulation were evaluated in pH 7.4 (Fig. 4**)**. The release follows a biphasic profile, characterized by a rapid initial burst (releasing 40% of the drug in 10 h), and followed by a second stage in which few changes were recorded. This two-phase release behavior has been reported for solid lipid nanoparticles (Nabi-Meibodi et al., 2013; Sun, Bi, Chan, Sun, Zhang & Zheng, 2013). The attached drug in the exterior shell and on the particle surface is related to burst release, while the drug that has been encapsulated into the lipid core is released in a sustained manner. This phenomenon was consistent with supposition of drug loading and physical characteristics. On the other hand, HA-VRS-SLNs exhibited a slightly lower release pattern in whole time points. HA layer plays a role as a barrier that could restrict the dispersion of drug to media.

### 3.4. Intracellular uptake study

Three cell lines present different expression of CD44 receptors (Ghosh, Neslihan Alpay & Klostergaard, 2012; Qhattal & Liu, 2011). To evaluate the intracellular uptake of formulations and the role of CD44 expression on cell surface, the intensity of incorporated dye was visualized and quantified using fluorescence microscopy and flow cytometry (NBD-PC labeled SLNs and HA-SLNs), respectively. Flow cytometry analysis was used to study the cellular uptake efficacy of HA-SLNs with or without pretreated HA. HA-SLNs showed a higher fluorescence shift compared to the controlled group and SLNs in SCC-7 cells, while a few right shifts were observed in the HA-SLNs after pretreatment with HA, indicating less cellular uptake into the SCC-7 cell line (Fig. 5**A**). This phenomenon clearly demonstrates the role of HA-CD44 interaction in terms of enhancing cellular uptake. In contrast, degree of cellular internalization of SLNs into MCF-7 cells after incubation for 30 min was slightly higher than that of HA-SLNs due to possible interaction between positive charge of SLN and negative charge of cell membrane (Fig. 5**B**). This result demonstrates the capacity of HA-SLNs to penetrate high overexpressed CD44 cells (SCC-7) through a process called receptor-mediated endocytosis; meanwhile, there is no significant difference for that system into low overexpressed CD44 cells (MCF-7) (Qhattal & Liu, 2011).

The internalization of SLNs and HA-SLNs was further visualized by confocal laser scanning microscope (CLSM). As shown in Fig. 6, similar results were obtained and agreed with flow cytometry data. In SCC-7 cells, the fluorescence intensity of HA-SLNs was higher than that of SLNs in SCC-7 cells, however, it was reduced by pretreatment with HA, which indicated that surface decoration with HA enhanced cellular uptake of SLNs based on CD44-mediated internalization. In addition, cellular uptake of HA-SLNs in MCF-7 cells was slightly lower than that of SLNs, suggesting that an affinity for CD44 may influence the efficient delivery of payloads.

### 3.5. In vitro cytotoxicity

The efficacy of the formulations against cancer cells is indicated by their cytotoxicity. Fig. 7 shows cytotoxicity results for cancer cells incubated with five different formulations, including blank HA-SLNs, blank SLNs, free VRS, VRS-SLNs, and HA-VRS-SLNs at 0.5, 1.0, 2.5, 5.0, 12.5, 25.0, and 50.0 μg/ml drug concentrations. Blank HA-SLNs did not show any appreciable cytotoxicity throughout the entire range of concentrations and the cell viability

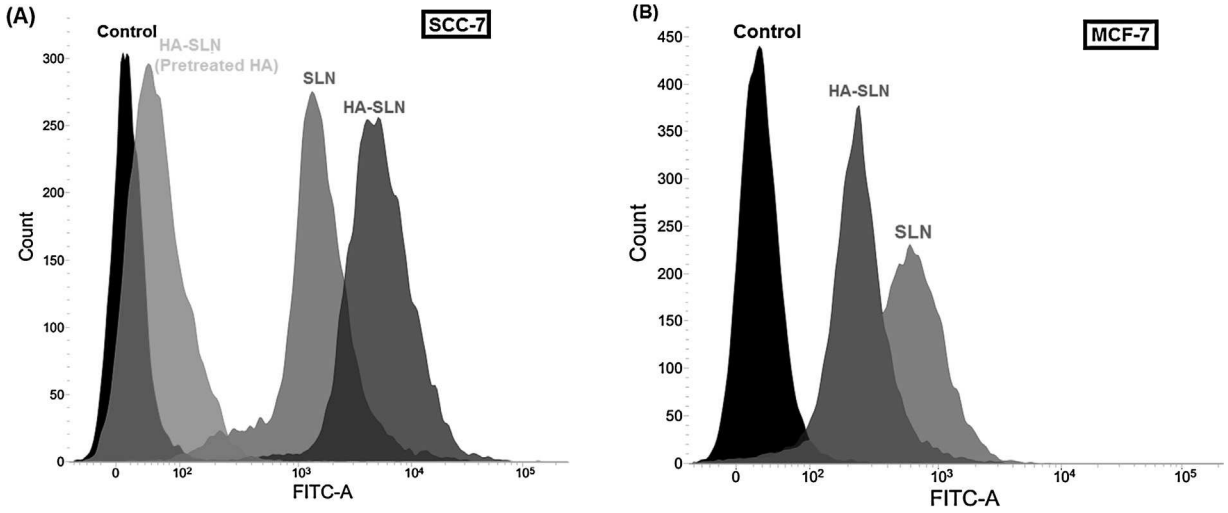


**Fig. 5.** Quantitative uptake of analysis by flow cytometry of SLNs, HA-SLNs and HA-SLNs pretreated with HA on (A) SCC-7 cells, and (B) MCF-7 cells.

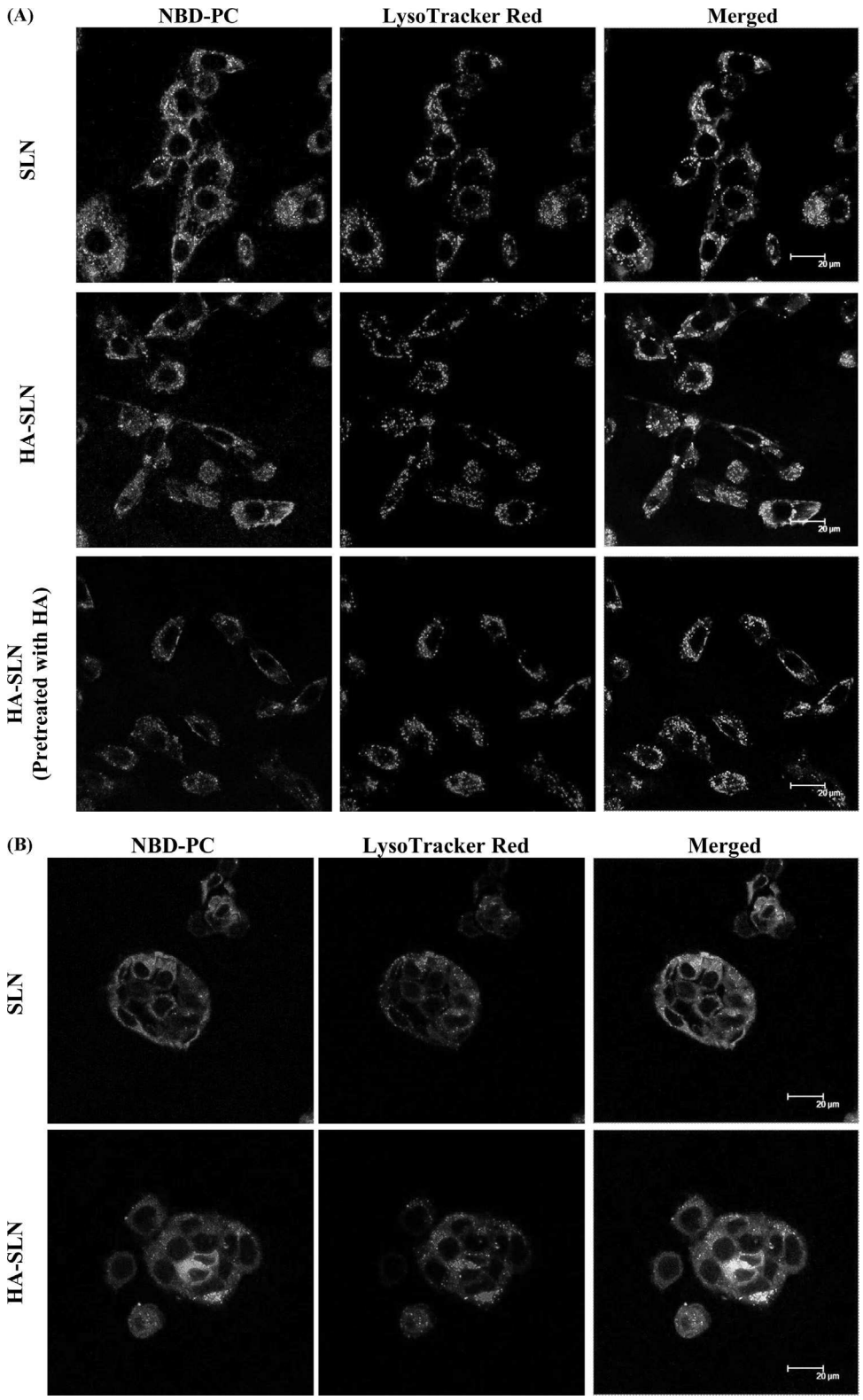


**Fig. 6.** Intracellular uptake of SLNs and HA-SLNs by confocal laser scan microscope images in (A) SCC-7 cells and (B) MCF-7 cells. SLNs and HA-SLNs containing NBD-PC (green) and Lysotracker Red (red) staining lysosome were used for this experiment. (For interpretation of the references to color in this figure legend, the reader is referred to the web version of this article.).

remained at more than 80% in all cell lines following 24 h exposure, demonstrating its biocompatible nature and tolerance (Petersen, Steiniger, Fischer, Fahr & Bunjes, 2011; Tran et al., 2014a). However, blank SLNs showed a slight cytotoxicity compared with blank HA-SLNs in all cell lines, which could be attributed by cationic DDAB on the surface of SLNs, leading to cell membrane destruction (Yang, Li, Li, Zhang, Feng & Zhang, 2013). In the case of blank HA-SLNs, the outer surface of the lipid was coated with HA so that HA can protect against disruption of cellular membranes, thereby reducing cytotoxicity versus the plain SLN itself. In

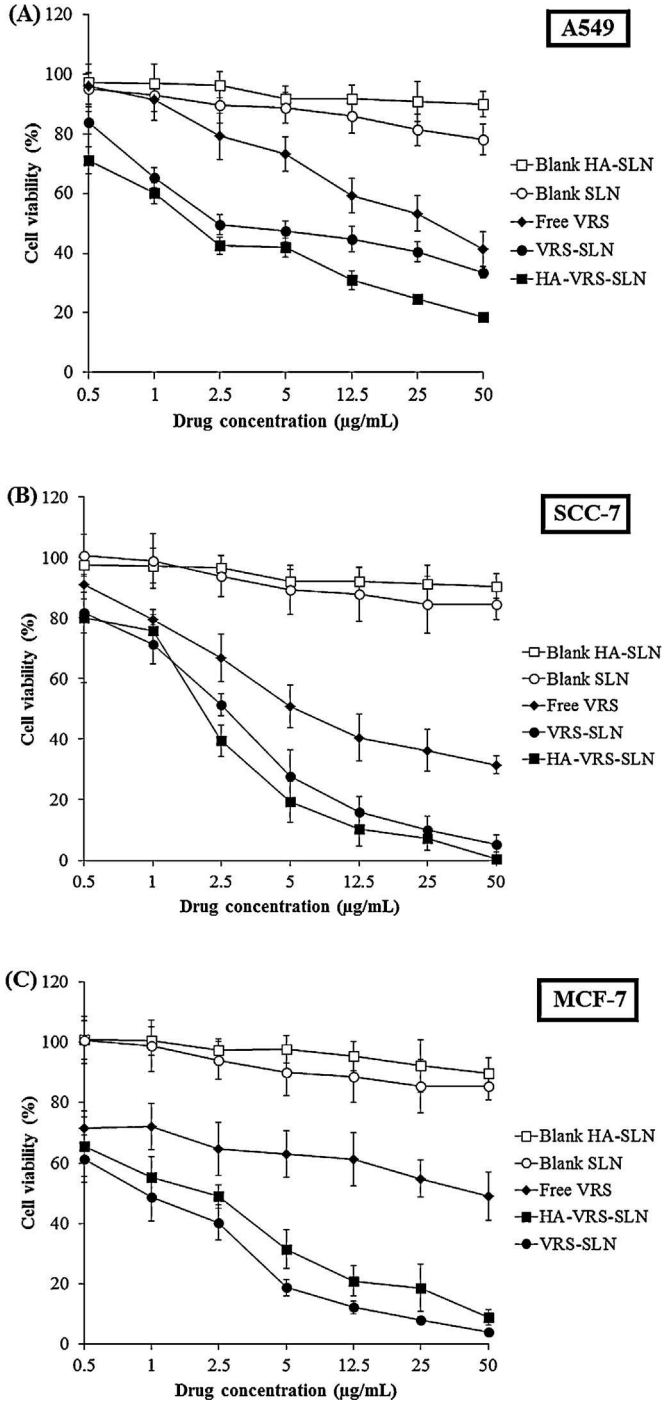


**Fig. 7.** In vitro cytotoxicity of blank SLNs, blank HA-SLNs, free VRS, VRS-SLNs and HA-VRS-SLNs after 24 h exposure in (A) A549, (B) SCC-7, and (C) MCF-7 cells. Data are expressed as the mean ± S.D. ($n = 8$).

addition, Fig. 7 showed that the cell-killing effects of VRS formulations were concentration-dependent. In all cell lines, in vitro antitumor activity of HA-VRS-SLNs was significantly higher than that of free VRS. The enhanced cytotoxic effect of HA-VRS-SLNs compared to free VRS may reflect the lipophilic nature of the carrier and enhanced intracellular uptake, by a rapid CD44 receptor-mediated endocytosis process (Ramasamy et al., 2013; Tran et al., 2014b). In particular, higher toxicity of HA-VRS-SLNs compared with VRS-SLNs was observed in A549 and SCC-7 cells with a high level of CD44 expression, while HA-VRS-SLNs did not show a better effect than VRS-SLNs MCF-7 cells with low CD44 levels. The good

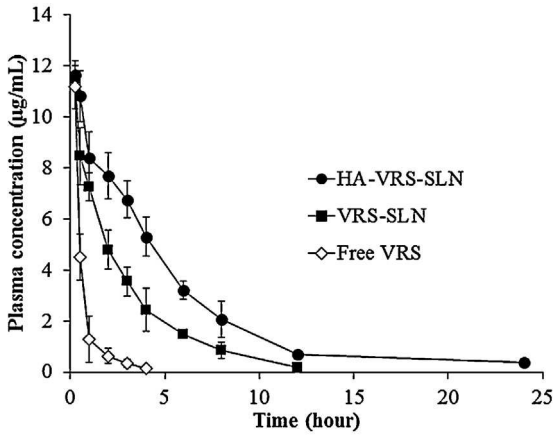


**Fig. 8.** Plasma concentration-time profile of VRS after intravenous administration at a dose of 10 mg/kg of free VRS (◊), VRS-SLNs (■) and HA-VRS-SLNs (•). Each value represents the mean ± S.D. ($n = 4$).

achievement of HA-VRS-SLNs could also be supposed by charge interaction between positive charge of SLNs and negative surface cell membrane after degradation of HA by HAase (Jiang et al., 2012). This result is consistent with *in vitro* cellular uptake studies by flow cytometric analyses and CLSM. Hence, development of the formulation could improve the therapeutic effect of VRS (Qhattal & Liu, 2011; Wei, Senanayake, Warren & Vinogradov, 2013).

### 3.6. Pharmacokinetic study

Fig. 8 shows the plasma concentration-time curves of VRS after intravenous administration of free drug suspension, VRS-SLNs and HA-VRS-SLNs. The mean plasma concentrations of VRS after IV injection of HA-VRS-SLNs were higher than those after injection of free VRS and VRS-SLNs. Owing to its hydrophobic property, free VRS was rapidly cleared from the blood stream. Half of VRS was eliminated after 0.65 ± 0.07 h, leading to mean residence time of only 0.77 ± 0.12 h, whereas $t_{1/2}$ and MRT of VRS-SLNs were 2.02 ± 0.52 and 3.20 ± 0.39 h, respectively (Table 1). However, among them, HA-VRS-SLNs showed the best performance with higher plasma concentration, longer half-life and MRT (4.55 ± 0.50, 6.26 ± 0.96 h). With the decrease in *in vivo* clearance, $AUC_{0-\infty}$ values of HA-VRS-SLNs (58.74 ± 6.19 μg.h/mL) were increased significantly ($p < 0.05$), compared with those of free VRS (16.62 ± 1.80 μg.h/mL) and VRS-SLNs (29.81 ± 3.84 μg.h/mL). As shown Fig. 8, VRS-SLNs improved drug state *in vivo*, but it faced clearance by the reticuloendothelial system (RES) due to a positive surface (Dobrovolskaia, Aggarwal, Hall & McNeil, 2008). Coating particles with long circulating agents such as PEG or HA are proposed as a solution to steric stabilization of vesicles and provide protection from opsonization, which is an essential desirable property in drug delivery (Peer, Karp, Hong, Farokhzad, Margalit & Langer, 2007). These results clearly indicated that the HA-coated VRS-SLNs would be successful in causing a reduction in dose and improvement in efficacy of VRS.

**Table 1**
Pharmacokinetic parameters of VRS in rats after intravenous administration of free VRS, VRS-SLNs, and HA-VRS-SLNs at a dose of 10 mg/kg.

| Parameter | Free VRS | VRS-SLNs | HA-VRS-SLNs |
|---|---|---|---|
| $C_{max}$ (μg/mL) | 11.17 ± 0.83 | 11.49 ± 0.11 | 11.67 ± 0.53 |
| $t_{1/2}$ (h) | 0.65 ± 0.07 | 2.02 ± 0.52[a] | 4.55 ± 0.50[a,b] |
| $AUC_{0-\infty}$ (μg.h/mL) | 16.62 ± 1.80 | 29.81 ± 3.84[a] | 58.74 ± 6.19[a,b] |
| MRT (h) | 0.77 ± 0.12 | 3.20 ± 0.39[a] | 6.26 ± 0.96[a,b] |

Data are expressed as the mean ± standard deviation ($n = 4$).
[a] $p < 0.05$, compared to the free drug.
[b] $p < 0.05$, compared to VRS-SLNs.

## 4. Conclusions

In this study, hyaluronic acid was successfully attached onto the surface of cationic SLNs by electrostatic attraction. The resultant particles were spherical in shape, uniform in size with a visually clear outer shell. HA-VRS-SLNs exhibited favorable characteristics that suggested their capability for efficient drug delivery and targeting. First, VRS was released slowly in order to maintain drug concentration in control, leading to reduced toxicity on normal cells. The HA-VRS-SLNs penetrated rapidly into cancer cells, especially on high level CD44 over-expression cells. In addition, the better performance of HA-VRS-SLNs clarified the role of HA in selective targeting to tumor cells. As expected, the HA-VRS-SLNs showed more potency in inhibiting the growth of all cancer cells: A549, SCC7, and MCF-7, compared to that for the VRS and VRS-SLNs. Finally, due to a hydrophilic and negative charge surface, HA-VRS-SLNs stayed longer in blood circulation and prolonged therapeutic drug concentration, which gave the drug a greater chance of reaching the tumor area. Taken together, our data indicated that HA-VRS-SLNs could be successfully developed as a targetable drug delivery system with high bioavailability.

## Acknowledgments

This research was supported by the National Research Foundation of Korea (NRF) grant funded by the Ministry of Education, Science and Technology (No. 2012R1A2A2A02044997 and No. 2012R1A1A1039059).

## References

Bhushan, S., Kakkar, V., Pal, H. C., Guru, S. K., Kumar, A., Mondhe, D., et al. (2012). Enhanced anticancer potential of encapsulated solid lipid nanoparticles of TPD: A novel triterpenediol from Boswellia serrata. *Molecular Pharmaceutics*, *10*(1), 225–235.

Bolden, J. E., Peart, M. J., & Johnstone, R. W. (2006). Anticancer activities of histone deacetylase inhibitors. *Nature Rreviews Drug Discovery*, *5*(9), 769–784.

Cai, Y., Yap, C., Wang, Z., Ho, P., Chan, S., Ng, K., et al. (2010). Solubilization of vorinostat by cyclodextrins. *Journal of Clinical Pharmacy and Therapeutics*, *35*(5), 521–526.

Choo, Q., Ho, P., & Lin, H. (2008). Histone deacetylase inhibitors: New hope for rheumatoid arthritis? *Current Pharmaceutical Design*, *14*(8), 803–820.

Dobrovolskaia, M. A., Aggarwal, P., Hall, J. B., & McNeil, S. E. (2008). Preclinical studies to understand nanoparticle interaction with the immune system and its potential effects on nanoparticle biodistribution. *Molecular Pharmaceutics*, *5*(4), 487–495.

Ghosh, S. C., Neslihan Alpay, S., & Klostergaard, J. (2012). CD44: A validated target for improved delivery of cancer therapeutics. *Expert Opinion on Therapeutic Targets*, *16*(7), 635–650.

Jiang, T., Zhang, Z., Zhang, Y., Lv, H., Zhou, J., Li, C., et al. (2012). Dual-functional liposomes based on pH-responsive cell-penetrating peptide and hyaluronic acid for tumor-targeted anticancer drug delivery. *Biomaterials*, *33*(36), 9246–9258.

Kelly, W. K., O'Connor, O. A., Krug, L. M., Chiao, J. H., Heaney, M., Curley, T., et al. (2005). Phase I study of an oral histone deacetylase inhibitor, suberoylanilide hydroxamic acid, in patients with advanced cancer. *Journal of Clinical Oncology*, *23*(17), 3923–3931.

Lee, M.-K., Lim, S.-J., & Kim, C.-K. (2007). Preparation, characterization and in vitro cytotoxicity of paclitaxel-loaded sterically stabilized solid lipid nanoparticles. *Biomaterials*, *28*(12), 2137–2146.

Luan, J., Zhang, D., Hao, L., Qi, L., Liu, X., Guo, H., et al. (2014). Preparation, characterization and pharmacokinetics of Amoitone B-loaded long circulating nanostructured lipid carriers. *Colloids and Surfaces B: Biointerfaces*, *114*, 255–260.

Marks, P. A., & Breslow, R. (2007). Dimethyl sulfoxide to vorinostat: development of this histone deacetylase inhibitor as an anticancer drug. *Nature Biotechnology*, *25*(1), 84–90.

Martins, S. M., Sarmento, B., Nunes, C., Lúcio, M., Reis, S., & Ferreira, D. C. (2013). Brain targeting effect of camptothecin-loaded solid lipid nanoparticles in rat after intravenous administration. *European Journal of Pharmaceutics and Biopharmaceutics*, *85*(3, Part A), 488–502.

Mohamed, E. A., Zhao, Y., Meshali, M. M., Remsberg, C. M., Borg, T. M., Foda, M., et al. (2012). Vorinostat with sustained exposure and high solubility in poly (ethylene glycol)-b-poly (dl-lactic acid) micelle nanocarriers: Characterization and effects on pharmacokinetics in rat serum and urine. *Journal of Pharmaceutical Sciences*, *101*(10), 3787–3798.

Nabi-Meibodi, M., Vatanara, A., Najafabadi, A. R., Rouini, M. R., Ramezani, V., Gilani, K., et al. (2013). The effective encapsulation of a hydrophobic lipid-insoluble drug in solid lipid nanoparticles using a modified double emulsion solvent evaporation method. *Colloids and Surfaces B: Biointerfaces*, *112*(0), 408–414.

Peer, D., Karp, J. M., Hong, S., Farokhzad, O. C., Margalit, R., & Langer, R. (2007). Nanocarriers as an emerging platform for cancer therapy. *Nature Nanotechnology*, *2*(12), 751–760.

Petersen, S., Steiniger, F., Fischer, D., Fahr, A., & Bunjes, H. (2011). The physical state of lipid nanoparticles influences their effect on in vitro cell viability. *European Journal of Pharmaceutics and Biopharmaceutics*, *79*(1), 150–161.

Qhattal, H. S. S., & Liu, X. (2011). Characterization of CD44-mediated cancer cell uptake and intracellular distribution of hyaluronan-grafted liposomes. *Molecular Pharmaceutics*, *8*(4), 1233–1246.

Ramasamy, T., Tran, T. H., Cho, H. J., Kim, J. H., Kim, Y. I., Jeon, J. Y., et al. (2013). Chitosan-based polyelectrolyte complexes as potential nanoparticulate carriers: Physicochemical and biological characterization. *Pharmaceutical Research*, 1–13.

Ramasamy, T., Tran, T. H., Choi, J. Y., Cho, H. J., Kim, J. H., Yong, C. S., et al. (2014). Layer-by-layer coated lipid–polymer hybrid nanoparticles designed for use in anticancer drug delivery. *Carbohydrate Polymers*, *102*(0), 653–661.

Raza, K., Singh, B., Singal, P., Wadhwa, S., & Katare, O. P. (2013). Systematically optimized biocompatible isotretinoin-loaded solid lipid nanoparticles (SLNs) for topical treatment of acne. *Colloids and Surfaces B: Biointerfaces*, *105*(0), 67–74.

Rivkin, I., Cohen, K., Koffler, J., Melikhov, D., Peer, D., & Margalit, R. (2010). Paclitaxel-clusters coated with hyaluronan as selective tumor-targeted nanovectors. *Biomaterials*, *31*(27), 7106–7114.

Strobl, J. S., Nikkhah, M., & Agah, M. (2010). Actions of the anti-cancer drug suberoylanilide hydroxamic acid (SAHA) on human breast cancer cytoarchitecture in silicon microstructures. *Biomaterials*, *31*(27), 7043–7050.

Sun, H., Benjaminsen, R. V., Almdal, K., & Andresen, T. L. (2012). Hyaluronic acid immobilized polyacrylamide nanoparticle sensors for CD44 receptor targeting and pH measurement in cells. *Bioconjugate Chemistry*, *23*(11), 2247–2255.

Sun, J., Bi, C., Chan, H. M., Sun, S., Zhang, Q., & Zheng, Y. (2013). Curcumin-loaded solid lipid nanoparticles have prolonged in vitro antitumour activity, cellular uptake and improved in vivo bioavailability. *Colloids and Surfaces B: Biointerfaces*, *111*(0), 367–375.

Tran, T. H., Ramasamy, T., Cho, H. J., Kim, Y. I., Poudel, B. K., Choi, H.-G., et al. (2014). Formulation and optimization of raloxifene-loaded solid lipid nanoparticles to enhance oral bioavailability. *Journal of Nanoscience and Nanotechnology*.

Tran, T. H., Ramasamy, T., Truong, D. H., Shin, B. S., Choi, H.-G., Yong, C. S., et al. (2014). Development of vorinostat-loaded solid lipid nanoparticles to enhance pharmacokinetics and efficacy against multidrug resistant cancer cells. *Pharmaceutical Research*.

Venishetty, V. K., Komuravelli, R., Kuncha, M., Sistla, R., & Diwan, P. V. (2013). Increased brain uptake of docetaxel and ketoconazole loaded folate-grafted solid lipid nanoparticles. *Nanomedicine: Nanotechnology, Biology and Medicine*, *9*(1), 111–121.

Wei, X., Senanayake, T. H., Warren, G., & Vinogradov, S. V. (2013). Hyaluronic acid-based nanogel–drug conjugates with enhanced anticancer activity designed for the targeting of CD44-positive and drug-resistant tumors. *Bioconjugate Chemistry*, *24*(4), 658–668.

Yang, X.-y., Li, Y.-x., Li, M., Zhang, L., Feng, L.-x., & Zhang, N. (2013). Hyaluronic acid-coated nanostructured lipid carriers for targeting paclitaxel to cancer. *Cancer letters*, *334*(2), 338–345.

# Formation of ion pairing as an alternative to improve encapsulation and anticancer activity of all-trans retinoic acid loaded in solid lipid nanoparticles

**Article** *in* International Journal of Nanomedicine · December 2012

DOI: 10.2147/IJN.S38953 · Source: PubMed



**8 authors**, including:

Guilherme Carneiro
Universidade Federal dos Vales do Jequitinhonha e Mucuri
**23** PUBLICATIONS **251** CITATIONS

SEE PROFILE

Elton Luiz Silva
Federal University of Minas Gerais
**5** PUBLICATIONS **74** CITATIONS

SEE PROFILE

Elaine Maria Souza-Fagundes
Federal University of Minas Gerais
**96** PUBLICATIONS **1,773** CITATIONS

SEE PROFILE

Natássia Corrêa
Universidade Federal de Uberlândia (UFU)
**7** PUBLICATIONS **103** CITATIONS

SEE PROFILE

International Journal of Nanomedicine

Dovepress
open access to scientific and medical research

Open Access Full Text Article

ORIGINAL RESEARCH

# Formation of ion pairing as an alternative to improve encapsulation and anticancer activity of all-trans retinoic acid loaded in solid lipid nanoparticles

Guilherme Carneiro[1]
Elton Luiz Silva[1]
Layssa Alves Pacheco[1]
Elaine Maria de Souza-Fagundes[2]
Natássia Caroline Resende Corrêa[3]
Alfredo Miranda de Goes[3]
Mônica Cristina de Oliveira[1]
Lucas Antônio Miranda Ferreira[1]

[1]Department of Pharmaceutics, Faculty of Pharmacy, Federal University of Minas Gerais, Belo Horizonte, Brazil; [2]Department of Physiology and Biophysics, Institute of Biological Sciences, Federal University of Minas Gerais, Belo Horizonte, Brazil; [3]Department of Biochemistry and Immunology, Institute of Biological Sciences, Federal University of Minas Gerais, Belo Horizonte, Brazil

Correspondence: Lucas Antônio Miranda Ferreira
Department of Pharmaceutics, Faculty of Pharmacy, Federal University of Minas Gerais (UFMG), Av Antônio Carlos, 6627, Campus Pampulha, CEP 31270-901, Belo Horizonte, Minas Gerais, Brazil
Tel +55 31 3409 6939
Fax +55 31 3409 6830
Email lucas@farmacia.ufmg.br

**Abstract:** This work aims to develop solid lipid nanoparticles (SLNs) loaded with retinoic acid (RA) to evaluate the influence of two lipophilic amines, stearylamine (SA) and benethamine (BA), and one hydrophilic, triethylamine (TA), on drug-encapsulation efficiency (EE) and cytotoxicity in cancer cell lines. The SLNs were characterized for EE, size, and zeta potential. The mean particle size decreased from 155 ± 1 nm (SLNs without amine) to 104 ± 4, 95 ± 1, and 96 ± 1 nm for SLNs prepared with SA, BA, and TA, respectively. SA-RA-loaded SLNs resulted in positively charged particles, whereas those with TA and BA were negatively charged. The EEs were significantly improved with the addition of the amines, and they increased from 36% ± 6% (without amine) to 97% ± 2%, 90% ± 2%, and 100% ± 1% for SA, TA, and BA, respectively. However, stability studies showed higher EE for BA-RA-loaded SLNs than TA-RA-loaded SLNs after 30 days. The formulations containing SA loaded or unloaded (blank SLNs) with RA were cytotoxic in normal and cancer cell lines. In contrast, the blank SLNs containing TA or BA did not show cytotoxicity in human breast adenocarcinoma cells (MCF-7), while RA-loaded SLNs with the respective amines were significantly more cytotoxic than free RA. Furthermore, the cytotoxicity of BA-RA-loaded SLNs was significantly higher than TA-RA-loaded SLNs. These findings are in agreement with the data obtained in the evaluation of subdiploid DNA content and cell-cycle analysis, which showed better anticancer activity for BA-RA-loaded SLNs than TA-RA-loaded SLNs and free RA. Taken together, these findings suggest that the BA-RA-loaded SLN formulation is a promising alternative for the intravenous administration of RA in the treatment of cancer.

**Keywords:** solid lipid nanoparticles, all-trans retinoic acid, cancer, treatment, antitumor activity, ion pairing

## Introduction

Vitamin A and its derivatives have the ability to reduce tumor growth and to induce apoptosis and differentiation in several types of cancer. In particular, all-trans retinoic acid (RA) has been studied for the treatment of cancer, including leukemia and breast cancer. The action of RA is attributed to its binding to the nuclear receptors, retinoic acid receptors, and retinoid X receptors, which regulate a variety of genes. RA can generally block the cell cycle in the G1 phase, causing cell proliferation inhibition and apoptosis.[1] The most effective clinical use of RA for human diseases was demonstrated in the treatment of acute promyelocytic leukemia.[2,3]

In clinical trials, RA has been given to cancer patients by oral administration. However, the bioavailability of oral RA has been considered low and quite variable.[4]

submit your manuscript | www.dovepress.com
Dovepress
http://dx.doi.org/10.2147/IJN.S38953

Moreover, continuous treatment with oral RA has been associated with progressive reduction of plasma concentrations, potentially to levels below those required to carry out its effect, probably due to the induced cytochrome P-450-dependent metabolism of RA.[5] Whereas these factors limit the clinical use of oral RA, an intravenous formulation could circumvent this problem.

RA, a hydrophobic drug with an octanol/water partition coefficient log of 4.6,[6] has poor aqueous solubility, and this can be a great disadvantage for endovenous administration. Some efforts have been made to enable intravenous administration of RA using nanocarriers, and a number of previous publications demonstrated that nanoparticles loaded with RA have significant influence over cancer cell viability.[7] In addition, lipid nanocarriers such as liposomes, nanoemulsions, and solid lipid nanoparticles (SLNs) have also been used.[8–10]

Among the advantages associated with SLNs are, most notably, the fact that their production is easily transposed to an industrial scale, as they do not require the use of organic solvents. In addition, compared with the nanoemulsions, which are prepared with liquid lipids, SLNs have more potential for controlled release, due to their solid matrix.[11–13] However, the RA encapsulation in SLNs is usually low[14] unless a high surfactant/lipid ratio is used.[15,16] This favors the drug location at the interface because of RA amphiphilicity,[17] thereby reducing the benefits obtained by the encapsulation in lipid matrix (increased stability, controlled release, and targeting effect).

We previously reported that the in situ formation of an ion pairing between RA, a lipophilic acid (Figure 1A), and different amines provides an interesting alternative to increased RA encapsulation in SLNs. Among the tested amines, stearylamine (SA) (Figure 1C), a lipophilic amine, provided the highest encapsulation.[18,19] These previous investigations were performed aiming for the development and evaluation of formulations for the topical treatment of acne. We hypothesized that SLNs loaded with RA, and different amines could be an interesting alternative for enabling intravenous administration of RA for cancer treatment. In the present study, we aimed to develop RA-loaded SLNs for parenteral administration, evaluating the influence of three amines: two lipophilic amines (SA and benethamine [BA]) (Figure 1B) and a hydrophilic one (triethylamine [TA]) (Figure 1D). The in vitro anticancer activity of SLNs loaded with RA and SA, TA, or BA was investigated against different cancer cell lines.

# Materials and methods

## Materials

Retinoic acid (RA), Compritol® 888 ATO (glyceryl behenate, mixture of mono-, di-, and triacylglycerols of behenic acid [$C_{22}$]) and Super Refined Tween 80™ (Polysobarte 80) were kindly provided by Basf (Ludwigshafen, Germany), Gattefossé (Lyon, France), and Croda Inc (Edison, NJ, USA), respectively. SA (octadecylamine), cholesterol, TA, and BA were purchased from Sigma-Aldrich (St Louis, MO, USA).

For in vitro studies, the Roswell Park Memorial Institute medium (RPMI) 1640 was obtained from Sigma-Aldrich; Dulbecco's modified Eagle's medium, fetal bovine serum, 3-(4,5-dimethylthiazol-2-yl)-2,5-diphenyl tetrazolium bromide (MTT), and staurosporine were purchased from Gibco (Life Technologies, Carlsbad, CA, USA).

The following cancer cell lines were used: Jurkat (immortalized line of T lymphocyte) was provided by Gustavo Amarante-Mendes (São Paulo University, São Paulo, Brazil). HCT-116 (colorectal carcinoma) and MCF-7 (human breast adenocarcinoma) cells were purchased from American Type Culture Collection (ATCC) (Manassas, VA, USA). All other chemicals were of analytical grade.

## Preparation of SLNs

SLNs were prepared by the hot melting homogenization method using an emulsification-ultrasound.[19] The

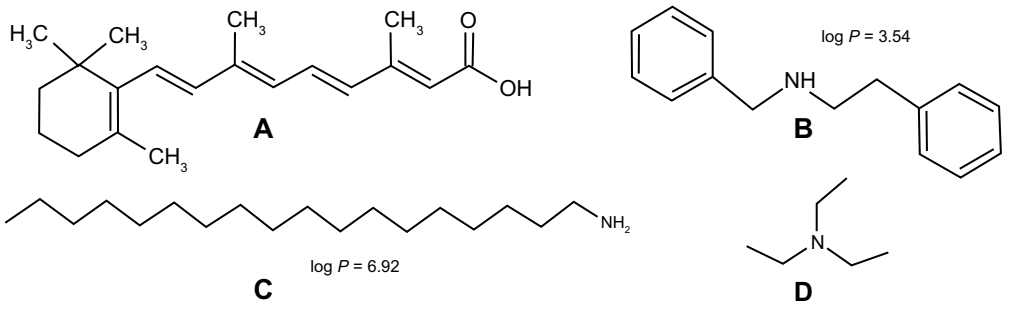


**Figure 1** Chemical structure of RA (**A**), benethamine (**B**), stearylamine (**C**), and triethylamine (**D**).
**Abbreviation:** RA, all-trans retinoic acid.

composition of the SLNs has previously been described, but with some modifications.[19] Considering the intended use of SLNs (intravenous administration), Tween 80™ was selected as surfactant. Briefly (batch 20 mL), the oily phase, composed of Compritol (400 mg), cholesterol (40 mg), Tween 80™ (300 mg), RA (10 mg), and the aqueous phase were heated separately to 85°C. Next, the aqueous phase was gently dropped onto the oily phase with constant agitation, at 8000 rpm in an Ultra Turrax T-25 homogenizer (Ika Labortechnik, Staufen, Germany). This emulsion was immediately submitted to the high-intensity probe sonication (20% amplitude) for 10 minutes, using a high-intensity ultrasonic processor (CPX 500 model; Cole-Palmer Instruments, East Bunker Court Vernon Hills, IL, USA). The influence of the in situ formation of an ion pairing between RA and amines was investigated. The SA or BA, and TA were selected as lipophilic and hydrophilic amines, respectively (RA/amine molar ratio was 1/2). The pH of the SLNs containing the amines was adjusted to 7.0 with a solution of 0.01 M HCl (Digimed DM 20, Santo Amaro, São Paulo, Brazil).

## Particle size analysis

The mean particle diameter of SLNs in the dispersion was determined by unimodal analysis through dynamic light scattering using a Zetasizer 3000HSA (Malvern Instruments, Malvern, UK), at a fixed angle of 90° and at 25°C. The SLN dispersions were diluted in distilled and filtered water (cellulose ester membrane, 0.45 μM, Millipore, Billerica, MA) up to a count rate of 50 to 300 Kcps (1000 counts per second). The data reported were particle size, evaluated as the intensity obtained from three repeat measurements, and the polydispersity index.[19]

## Zeta potential

Zeta potential measurements were carried out by the electrophoretic mobility determination at 90° and 25°C. Before the measurements, SLN dispersions were diluted in filtered 1 mM NaCl solution (cellulose ester membrane, 0.45 mm, Millipore) up to a count rate of 100 to 1000 Kcps. All measurements were performed in triplicate using a Zetasizer 3000HSA (Malvern Instruments).

## Drug-encapsulation efficiency

Encapsulation efficiency (EE) for RA in SLNs was determined according to the method previously described.[19] This method was based on the determination of RA concentration in the SLNs before (total RA) and after filtration (cellulose ester membrane, 0.45 μM, Millipore). The RA crystals, usually measuring a few micrometers across, present characteristic forms and can be easily distinguished from SLNs.[14] RA concentration in the external aqueous phase of the SLNs was determined by ultrafiltration method (Amicon® 100 k, Millipore) with a 100 kDa molecular weight cutoff membrane. RA concentration in the aqueous phase was negligible, owing to its low solubility in water.[15]

RA concentration in SLNs (before and after filtration) or in the aqueous phase was determined according to the method described by Castro et al.[18] Briefly, an aliquot of the SLN dispersion was dissolved in tetrahydrofuran and later diluted in a mixture of acetonitrile, distilled water, and phosphoric acid (80:19.9:0.1). This mixture keeps the RA in solution (dissolved), but causes lipid precipitation. This dispersion was filtered in a 0.45 μM Millex HV filter (Millipore) and analyzed by HPLC. EE was calculated using the following formula: EE (%) = (filtered RA/total RA) × 100.

To investigate the influence of the amines on stability (RA retention in lipid matrix), two SLN formulations loaded with lipophilic BA or hydrophilic TA were prepared. The two SLN formulations were injected into 10 mL glass containers within a nitrogen atmosphere and were stored at 4°C. Sampling aliquots were withdrawn at 30 days, and the EE was determined as previously described.

High performance liquid chromatography (HPLC) consisted of a Waters 515 HPLC Pump (Milford, MA), a Waters 717 Plus Auto-sampler, and a photodiode array detector (Waters 2996). A $C_{18}$ reverse-phase column (125 mm of length, 4 mm of width, and particles of 5 μm) (LichroCart 125–4, Merck, Darmstadt, Germany) was used. The mobile phase was a mixture of acetonitrile, distilled water, and phosphoric acid (80:19.9:0.1). The detection was carried out at 340 nm, with a flow rate of 1.0 mL/minute and 20 μL of sample. The five-point (0.25, 0.5, 1.0, 2.0, and 5.0 μg/mL) linear regression analysis resulted in the following linear equation: $y = -2435 + 137200 \times (r = 0.9998)$.

## Cell cultures

Cell viability studies were conducted against both normal and cancer cells. Cancer cell lines (Jurkat, HL-60, HCT-116, and MCF-7) were cultured in RPMI or Dulbecco's modified Eagle's medium containing fetal bovine serum (10%), 200 mM glutamine, and antibiotics (100 μg/mL streptomycin and 100 UI/mL penicillin). All cultures were kept in a humidified incubator with 5% $CO_2$ at 37°C. Normal cells (peripheral blood mononuclear cells; PBMCs) were obtained through agreement with the Minas Gerais Hematology and Hemotherapy Center Foundation – HEMOMINAS –

(protocol n° 105/2004) from healthy adult volunteers of both sexes by centrifugation of heparinized venous blood over a Ficoll cushion. PBMCs were collected from the interphase after Ficoll separation and washed three times in RPMI before further processing.[20] All PBMC cultures were carried out in RPMI medium, supplemented with 5% (v/v) heat-inactivated, pooled AB sera, and 2 mM L-glutamine. An antibiotic/antimicotic solution containing 1000 U/mL penicillin, 1000 μg/mL streptomycin, and 25 μg/mL fungizone was added to control fungal and bacterial contamination.

## Analysis of cell viability

Cell proliferation was measured by MTT assay based on the reduction of tetrazolium salt to formazan crystals by living cells.[21] Briefly, aliquots containing $7.0 \times 10^3$ (MCF-7), $9 \times 10^3$ (HL60), $1.8 \times 10^4$ (Jurkat and HCT-116), or $3.6 \times 10^4$ (PBMC) cells/well were seeded into 96-well plates. After 24 hours of incubation at 37°C and 5% $CO_2$, freshly prepared solutions of free RA and SLNs were added to the wells (RA concentration ranged from 0.78 μM to 100 μM). Free RA was dissolved in absolute ethanol (4 mM) prior to dilution. After 48 hours of incubation at 37°C and 5% $CO_2$, 20 μL of the 5 mg/mL MTT solution was added to each plate. Plates were incubated at 37°C for 4 hours, and then the medium was replaced by 200 μL of 0.04 M HCl solution in isopropanol. Cell viability was estimated by measuring the rate of mitochondrial reduction of MTT, determined by evaluating the absorbance of the converted dye at a wavelength of 595 nm. Absorbance values of the wells in which the cells were maintained in medium alone were considered as 100% of cell viability. Control groups included treatment with ethanol (negative control) and staurosporine (positive control). Cell viability was found to be 100% after treatment with negative control (ethanol), while staurosporine was effective in promoting cell-growth inhibition. Data were expressed as percentage of cell viability compared to the control (mean ± standard deviation [SD]). At least three independent experiments were performed.

## Subdiploid DNA content and cell-cycle analysis

A flow-cytometric DNA fragmentation assay was employed as a quantitative measure of subdiploid content and phases of the cell cycle.[22] MCF-7 cells were plated at a density of $5 \times 10^4$ cells/well on 24-well plates and treated with free RA, RA-loaded SLNs, or blank SLNs for 48 hours (RA concentration was 25 μM). After this time, cells were centrifuged at 200 g (gravities) for 5 minutes at room temperature, and the culture medium was aspirated off. The pellet was gently resuspended in 300 μL of hypotonic fluorochrome solution containing 0.5% Triton X-100 and 50 μg/mL propidium iodide. Cells were incubated in the dark at 4°C for 4 hours and analyzed with a Guava® EasyCyte™ 6-2L Base System cytometer (Millipore). Data analysis was performed with FlowJo™ 7.6.5 (Tree Star Inc, Ashland, OR, USA), to determine percentages of subdiploid content and phases of the cell cycle.

## Data analysis

Analysis of the cytotoxicity and cell-cycle studies were carried out using one-way ANOVA followed by Tukey's test. For all analyses, the difference was considered significant when the $P$ value was $<0.05$.

# Results

## Preparation and characterization of SLNs

The main characteristics of RA-loaded SLNs prepared with lipophilic (SA or BA) and hydrophilic (TA) amines are listed in Table 1. The mean particle size decreased from 155 ± 1 nm (SLNs without amine) to 104 ± 4 nm and 95 ± 1 for SLNs loaded with SA and BA lipophilic amines, respectively. Negatively charged particles were obtained for SLNs without amine (–30 ± 1 mV) and SLNs loaded with BA (zeta potential of –39 ± 0.2 mV). In contrast, using SA resulted in positively charged particles with a zeta potential of 20 ± 2 mV. These differences in particle charge can be explained by the fact that SA presents a higher potential for interfacial adsorption, in comparison to BA. In fact, the lipophilicity of SA is higher than that of BA (Figure 1). It is noteworthy that EE for RA in SLNs increased from 36% ± 6% (SLNs without amine) to 97% ± 2% and 100% ± 1% for SLNs loaded with SA and BA, respectively. Therefore, SA and BA promoted a significant increase of EE for RA in SLNs. A plausible explanation for the EE increase could be the formation of an ion pairing between RA and the lipophilic amines.

**Table 1** Influence of the amine type on the particle size, polydispersion index, zeta potential and EE of RA in SLNs

| Parameter | Without amine | SA | TA | BA |
|---|---|---|---|---|
| Mean diameter (nm) | 155 ± 1 | 104 ± 4 | 96 ± 1 | 95 ± 1 |
| Polydispersion index | 0.24 ± 0 | 0.24 ± 0 | 0.3 ± 0.1 | 0.24 ± 0.01 |
| Zeta potential (mV) | –30 ± 4 | 20 ± 2 | –33 ± 4 | –39 ± 0.2 |
| EE (%) | 36 ± 6 | 97 ± 2 | 90 ± 2 | 100 ± 1 |

**Note:** Data are shown as mean ± SD (n = 3).

**Abbreviations:** BA, benethamine; EE, encapsulation efficiency; RA, all-trans retinoic acid; SLN, solid lipid nanoparticle; SA, stearylamine; SD, standard abbreviation; TA, triethylamine.

The ion pairing increases the lipophilic properties of the drug, making its incorporation into the lipid matrix easier. These findings are in agreement with previous observations that showed that the loading capacity in SLNs is related to drug lipophilicity.[23,24]

For the SLNs prepared with TA, a reduction in the particle diameter to 96 ± 1 nm was also observed. These SLNs were negatively charged (zeta potential of –33 ± 4 mV), and this can be explained by the fact that interfacial adsorption of hydrophilic TA is unlikely. TA also promoted a significant increase in EE for RA in SLNs (90% ± 2%), when compared with SLNs without amine (Table 1). However, as shown in Figure 2, after 30 days of storage at 4°C, a dramatic decrease in EE for RA in RA-TA-loaded-SLNs was observed (from 90% ± 2% to 27% ± 0.1%). In significant contrast, the EE for BA-loaded SLNs was high immediately after preparation and remained constant after 30 days (98% ± 2%). These findings are in agreement with our previous data, which showed that it was possible to produce RA-loaded SLNs with high EE and stability by employing RA-amine ion pairing. Increasing the lipophilicity of the amine increases the drug-loading capacity in SLNs due to the increase in lipophilicity of the ion pair formed.[19]

## Cell viability studies

To investigate whether cytotoxicity of RA was affected by loading in SLNs containing amines, the cell viability assay using MTT was investigated in cancer and normal cells. First, the cell viability of SLNs loaded with lipophilic SA was assayed. Normal and human cancer cells were incubated with free RA, unloaded (blank) SLNs, or RA-SA-loaded SLNs and analyzed for their viability. The data obtained, expressed as cell viability (percentage), are shown in Figure 3. The lowest antitumor activity was observed for the free RA (cell viability was approximately 80%), independent of the cell lines evaluated. MCF-7 cells were more sensitive to free RA, while the Jurkat and HCT-116 cells were the least sensitive. In contrast, the activity of SA-RA-loaded SLNs was much higher than that observed for the free RA, with MCF-7 cells showing greater sensitivity, compared with other cancer cells. However, the cytotoxic effects of unloaded (blank) SLNs against tumor cells were also high. It is interesting to note that these cytotoxic effects were also observed against normal cells (PBMCs). The cytotoxicity of the blank SLNs was attributed to the presence of the cationic lipophilic SA. In fact, blank SLNs without SA were prepared and their cytotoxic effects against MCF-7 cells investigated. These effects had disappeared completely (data not shown). Considering that the MCF-7 cells were more sensitive to RA, these cells were selected for further studies.

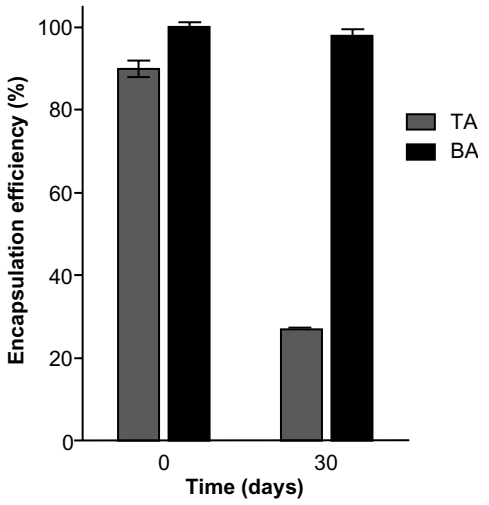


**Figure 2** Stability of encapsulation efficiency (EE) of RA in SLNs prepared with triethylamine (TA) or benethamine (BA).
**Note:** Data represent mean ± SD (n = 3).
**Abbreviations:** RA, all-trans retinoic acid; SD, standard deviation; SLN, solid lipid nanoparticle.

To investigate whether SLNs loaded with hydrophilic TA or lipophilic BA, which were used as amines for the in situ formation of an ion pairing with RA, would show the same pattern of activity, MCF-7 cancer cells were incubated with unloaded (blank) SLNs, RA-TA-loaded SLNs, RA-BA-loaded SLNs, or free RA and analyzed for their metabolic viability. The data obtained, expressed as percentage of MTT metabolism, are shown in Figure 4. Interestingly, blank SLNs loaded with TA or BA showed no inhibitory effect, with cell viability near 100%. These data demonstrate that blank SLNs loaded with TA or BA present negligible cytotoxicity, when compared with the blank SLNs loaded with SA, and they are a potential new alternative for development of formulations for intravenous administration of RA. In addition, RA-loaded SLNs containing BA or TA presented cytotoxic effects significantly higher than those observed for the free RA in all drug concentrations tested; a dose-dependent relationship between drug concentration and cell viability was clearly observed. The maximum reductions in cell viability for RA-TA-loaded SLNs, RA-BA-loaded SLNs, and free RA, observed at the concentration 100 μM, were 45% ± 5%, 34% ± 4%, and 71% ± 2%, respectively. The differences between BA-loaded SLNs and TA-loaded SLNs were significant.

## Subdiploid DNA content and cell-cycle analysis

In order to determine whether the improvement of the cytotoxic activity of RA after incorporation into BA-

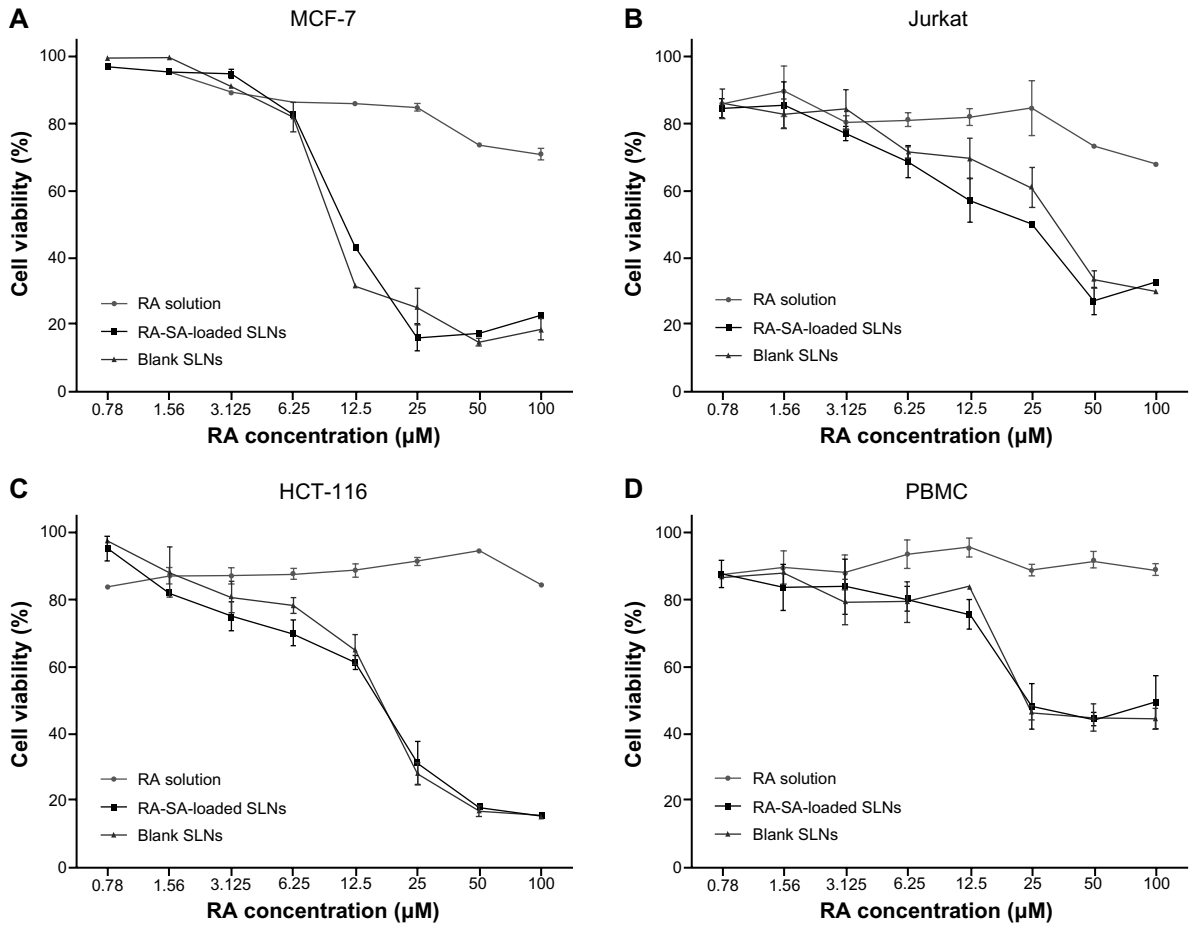


**Figure 3** Cell viability studies, as evaluated by MTT assay, of blank SLNs, RA-SA-loaded SLNs, and free RA in cancer and normal cells, MCF-7 (**A**), Jurkat (**B**), HCT-116 (**C**), and PBMCs (**D**), after 48 hours of exposure.

**Notes:** Data were expressed as mean ± SD of three independent experiments. The blank SLNs were diluted at the same proportion as RA-loaded SLNs.

**Abbreviations:** MTT, 3-(4,5-dimethylthiazol-2-yl)-2,5-diphenyl tetrazolium bromide; RA, all-trans retinoic acid; PBMC, peripheral blood mononuclear cells; SA, stearylamine; SD, standard deviation; SLN, solid lipid nanoparticle.

loaded SLNs was associated with alterations in cell-cycle progression and DNA fragmentation, we performed flow cytometry studies. We used the protocol described by Riccardi and Nicoletti,[22] that is based on the principle that apoptotic cells, among other typical features, are characterized by DNA fragmentation and, consequently, loss of nuclear DNA content. The use of a fluorochrome, such as propidium iodide, that is capable of binding and labeling DNA makes it possible to obtain a rapid and precise evaluation of cellular DNA content by flow-cytometric analysis and subsequent identification of hypodiploid cells. Representative histograms of DNA content after PI staining are shown in Figure 5. The data are summarized in Table 2. The increase in subdiploid DNA content was negligible for the treatment with RA-TA-loaded SLNs (0.5% ± 0.20%) and free RA (0.4% ± 0.05%), when compared with the control. After 48 hours of treatment, the subdiploid DNA content for RA-BA-loaded SLNs (6.1% ± 0.65%) was significantly increased, inducing DNA fragmentation 12 and 17 times higher than that observed for the RA-TA-loaded SLNs and free RA, respectively. Blank SLNs (with TA or BA) showed no significant increase in subdiploid content in comparison with the control. These data suggest that BA-containing SLNs show more advantages as carriers of RA than the TA-loaded SLNs, as observed in the improvement of their cytotoxic effects.

Data concerning the cell-cycle stage distribution clearly showed a significant increase in the $G_0/G_1$ phase after treatment with RA-loaded SLNs (73.0% ± 0.5% and 74% ± 0.6% for SLNs with TA and BA, respectively), when compared with the control (60.5% ± 1.0%). This increase was higher than that observed for the treatment with free RA (70.6% ± 0.5%). Also, the frequency of MCF-7 cells in the S-phase range of DNA content decreased. This reduction was more evident in SLNs with BA (8% ± 0.3%) than in SLNs with TA (12.4% ± 0.6%), when compared with the

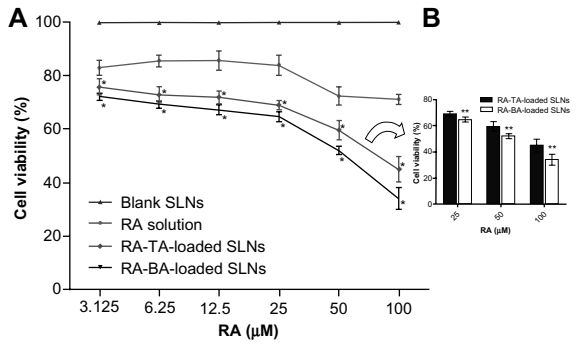


**Figure 4** Cell viability studies, as evaluated by MTT assay, of blank SLNs, RA-TA-loaded SLNs, RA-BA-loaded SLNs and free RA in MCF-7 cells after 48-hour exposure.

**Notes:** Data were expressed as mean ± SD of three independent experiments. The data for blank SLNs, which were diluted at the same proportion as RA-loaded SLNs, represent overlapping values for TA-based SLNs and BA-based SLNs. [a]Significant difference compared to free RA; [b]significant difference between TA-based SLNs and BA-based SLNs.

**Abbreviations:** MTT, 3-(4,5-dimethylthiazol-2-yl)-2,5-diphenyl tetrazolium bromide; BA, benethamine; RA, all-trans retinoic acid; SLN, solid lipid nanoparticle; TA, triethylamine.

control (14.8% ± 0.7%). Free RA also showed a significant decrease in the S-phase (10.8% ± 0.1%), which was revealed to be lower than that observed for the treatment with RA-BA-loaded SLNs. These findings are in agreement with previous observations that showed that RA treatment of MCF-7 cells induces G1 arrest before inducing apoptosis.[24,25]

## Discussion

SLNs have gained attention as particulate systems that improve the delivery of lipophilic drugs, such as RA, due to the high affinity of these molecules for the lipid matrix.[11,12] However, unexpectedly, the EE for RA in SLNs is usually low, and the in situ formation of an ion pairing between RA and an amine provides an interesting alternative to enhance the drug encapsulation.[19] Therefore, this work aimed to develop, characterize, and evaluate the in vitro antitumor activity of SLNs loaded with RA and different amines. Three amines were evaluated: one hydrophilic (TA) and two lipophilic amines (SA and BA).

Marked differences between formulations were observed when the data concerning the RA encapsulation in SLNs were evaluated. Our data clearly show that EEs was significantly increased in SLNs containing SA, TA, or BA, when compared with SLNs without amines. Comparing the amines, the data show that the EEs for RA in SLNs loaded with lipophilic amines (BA and SA) were higher than that observed for SLNs containing TA. In addition, the stability (drug retention) of SLNs loaded with lipophilic BA was much higher than that observed for SLNs containing TA. Although TA is considered a stronger base than BA or SA (the pKb value for TA is lower than that for other amines), the differences in

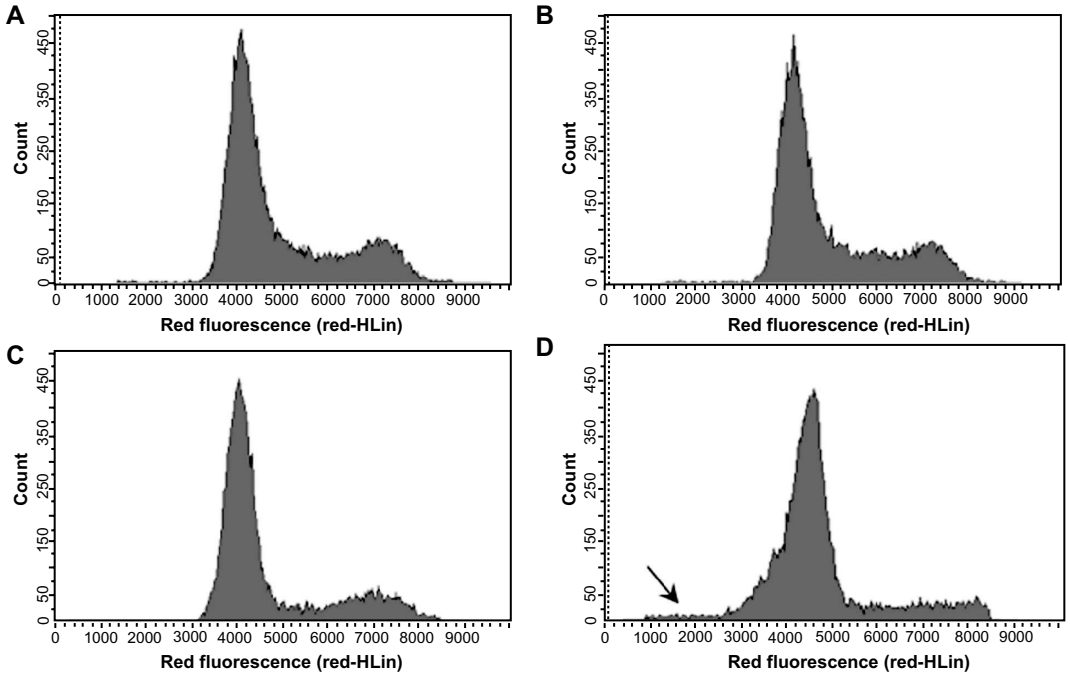


**Figure 5** DNA fluorescence histograms of PI-stained MCF-7 cells after 48 hours of incubation under various experimental conditions: medium alone (**A**), blank SLNs (**B**), free RA (**C**), or BA-RA-loaded SLNs (**D**).

**Notes:** RA was used at 25 μM. BA-RA-loaded SLNs induce cell-cycle arrest accompanied by reduction in the S phase in MCF-7 cells. Data from one representative experiment that represents 20,000 events (cells) are shown.

**Abbreviations:** BA, benethamine; PI, propidium iodide; RA, all-trans retinoic acid; SLN, solid lipid nanoparticle.

**Table 2** Effects of different treatments of MCF-7 cancer cells on DNA fragmentation and cell-cycle stage distribution

| Sample | Subdiploid content (%) | $G_0/G_1$ (%) | S (%) | $G_2/M$ (%) |
|---|---|---|---|---|
| Control | 0.2 ± 0.1 | 60.5 ± 1.0 | 14.8 ± 0.7 | 24.2 ± 0.4 |
| Free RA | 0.4 ± 0.1 | 70.6 ± 0.5 | 10.8 ± 0.1 | 16.2 ± 0.3 |
| **SLNs with TA** | | | | |
| Blank SLNs | 0.4 ± 0.2 | 64.0 ± 0.6 | 16.8 ± 0.0 | 17.5 ± 0.7 |
| RA-loaded SLNs | 0.5 ± 0.2 | 73.0 ± 0.5 | 12.4 ± 0.6 | 14.1 ± 0.3 |
| **SLNs with BA** | | | | |
| Blank SLNs | 0.7 ± 0.1 | 62.8 ± 0.8 | 17.1 ± 0.4 | 19.3 ± 1.0 |
| RA-loaded SLNs | 6.1 ± 0.7 | 73.8 ± 0.6 | 6.8 ± 0.2 | 13.3 ± 0.9 |

**Notes:** MCF-7 cells were treated with RA-loaded SLNs, free RA, and unloaded (blank) SLNs, as indicated in the methods section. Cell-cycle distributions were determined after 48 hours of treatment. The data are representative of three independent experiments. Mean ± SD is shown.

**Abbreviations:** BA, benethamine; RA, all-trans retinoic acid; SLN, solid lipid nanoparticle; SD, standard deviation; TA, triethylamine.

basicity among amines are relatively low. On the other hand, our data showed that RA retention in lipid matrix increases with the hydrophobicity of the counterion used for the ion pair formation, revealing that lipophilicity rather than basicity was the most relevant parameter. These findings are consistent with our previous observations, which showed that EE for RA in SLNs significantly increased when the lipophilicity of the amine increased, producing more-stable SLNs.[18] These findings demonstrate that the lipophilic amine triggered an intense interaction of RA with the lipid matrix.

Cytotoxic effects against both cancer and normal cells were investigated. It was clearly observed that in vitro antitumor activity of RA-SA-loaded SLNs was higher than that observed for free RA. Data for free RA compare with findings previously described.[25,26] However, cytotoxic effects for unloaded (blank) SLNs were also high against both cancer and normal cells. This phenomenon was attributed to the cationic lipid (SA), since blank SLNs without SA showed no cytotoxic effects against MCF-7 cells. These data are in agreement with previous findings, which demonstrated that cationic lipid-stabilized SLNs or liposomes show cytotoxic effects. The proposed mechanisms of the cytotoxicity are the electrostatic interactions of these cationic amphiphilic molecules, with the anionic phospholipids of the cell membrane leading to membrane damage.[27–29]

To reduce the toxicity, SLNs loaded with TA or BA were produced and tested in MCF-7 cells. Blank SLNs, which displayed negatively charged particles, revealed no cytoxicity against the tested cancer cells. In contrast, RA-loaded SLNs showed a remarkable increase in antitumor activity against the human breast cancer cell line MCF-7, in comparison with the free RA. The reduction in cell viability observed for BA-loaded SLNs were significantly higher than that observed for TA-loaded SLNs, and differences between the two formulations were even more prominent when the data for subdiploid DNA content were evaluated. Furthermore, it was observed that RA-loaded SLNs were able to decrease the frequency of MCF-7 cells in the S-phase and to accumulate cells in the $G_0/G_1$-phases. These effects were more pronounced than those observed for free RA and are consistent with data reported previously.[30,31]

Previous studies showed no significant increase in the anticancer activity of RA-loaded lipid nanocarriers when compared to free RA.[8,32] Su and colleagues[33] showed that the cytoxicity of RA-loaded tributyrin nanoemulsion against hepatic or colonic cancer cells was higher than that of free RA. However, the combination of RA with tributyrin, a prodrug of butyric acid, was reported to have synergistic anticancer effects.[34,35] Therefore, it is difficult to separate the effects of the combination of RA and tributyrin from those of drug encapsulation.

The present study reported for the first time a remarkable increase in anticancer activity of RA-BA-loaded SLNs in comparison with free RA. The in situ formation of an ion pairing between RA and BA favors drug retention in lipid matrix. After dilution of the nanoparticles in the culture medium, two opposing scenarios can occur: RA may be released (bound or not to the amine) or remain associated with the SLNs. If RA is released from SLNs as an ion pair, reverse ion exchange can occur, with ions from the culture medium substituting the counterions (amines), resulting in the reformation of the parent drug.[36] In this case, it would be expected that the activity of the SLNs was similar to that observed for the free RA. Considering that our data showed a higher activity for the SLNs, the most probable hypothesis is that RA remained associated with the lipid matrix of the SLNs after dilution in the medium, enabling improved drug uptake by the tumor cells.[37] Previous studies have reported enhanced – despite negatively charged particles – intracellular levels of anticancer drugs loaded in SLNs.[38]

Finally, studies have pointed out the important role RA plays in the control of metabolic diseases such as diabetes and obesity through its activation of the retinoid X receptor and its heterodimers pathways. Treatment with RA can reduce body weight and adiposity, and enhance glucose tolerance and insulin sensitivity.[39,40] To improve bioavailability, RA has been administered orally as an emulsion and subcutaneously as an oily solution. For novel formulations, the ion pair formation in SLNs can be explored as a strategy to improve the efficacy and bioavailability of RA in the treatment of obesity and diabetes.

## Conclusion

In summary, an SLN formulation loaded with RA, a lipophilic acid, and a lipophilic amine (BA) was designed and evaluated. It was possible to obtain high encapsulation efficiency (almost 100%) for RA in SLNs. Moreover, RA-BA-loaded SLNs promoted enhanced in vitro antitumor activity when compared to the free RA and other SLN formulations. These findings suggest that the RA-BA-loaded SLN formulation is a promising alternative for the administration of RA in the treatment of cancer.

## Acknowledgments

This study was supported by the Minas Gerais State Agency for Research and Development (FAPEMIG, Brazil) and by the Brazilian agencies CAPES and CNPq. The authors wish to thank Glenn Hawes from the American Language Program of the University of Georgia for editing this manuscript.

## Disclosure

The authors state no conflict of interest and have received no payment in preparation of this manuscript. All authors have approved the final article.

## References

1. Tang XH, Gudas LJ. Retinoids, retinoic acid receptors, and cancer. *Annu Rev Pathol*. 2011;6:345–364.
2. Niles RM. Signaling pathways in retinoid chemoprevention and treatment of cancer. *Mutat Res*. 2004;555(1–2):81–96.
3. Bushue N, Wan YJ. Retinoid pathway and cancer therapeutics. *Adv Drug Deliv Rev*. 2010;62(13):1285–1298.
4. Adamson PC, Pitot HC, Balis FM, Rubin J, Murphy RF, Poplack DG. Variability in the oral bioavailability of all-trans-retinoic acid. *J Natl Cancer Inst*. 1993;85(12):993–996.
5. Muindi JR, Frankel SR, Huselton C, et al. Clinical pharmacology of oral all-trans retinoic acid in patients with acute promyelocytic leukemia. *Cancer Res*. 1992;52(8):2138–2142.
6. Abdulmajed K, Heard CM. Topical delivery of retinyl ascorbate co-drug. 1. Synthesis, penetration into and permeation across human skin. *Int J Pharm*. 2004;280(1–2):113–124.
7. Chung KD, Jeong YI, Chung CW, Kim do H, Kang DH. Anti-tumor activity of all-trans retinoic acid-incorporated glycol chitosan nanoparticles against HuCC-T1 human cholangiocarcinoma cells. *Int J Pharm*. 2012;422(1–2):454–461.
8. Lim SJ, Lee MK, Kim CK. Altered chemical and biological activities of all-trans retinoic acid incorporated in solid lipid nanoparticle powders. *J Control Release*. 2004;100(1):53–61.
9. Chansri N, Kawakami S, Yamashita F, Hashida M. Inhibition of liver metastasis by all-trans retinoic acid incorporated into O/W emulsions in mice. *Int J Pharm*. 2006;321(1–2):42–49.
10. Kawakami S, Suzuki S, Yamashita F, Hashida M. Induction of apoptosis in A549 human lung cancer cells by all-trans retinoic acid incorporated in DOTAP/cholesterol liposomes. *J Control Release*. 2006;110(3):514–521.
11. Muller RH, Mader K, Gohla S. Solid lipid nanoparticles (SLN) for controlled drug delivery – a review of the state of the art. *Eur J Pharm Biopharm*. 2000;50(1):161–177.
12. Jenning V, Lippacher A, Gohla SH. Medium scale production of solid lipid nanoparticles (SLN) by high pressure homogenization. *J Microencapsul*. 2002;19(1):1–10.
13. Joshi MD, Muller RH. Lipid nanoparticles for parenteral delivery of actives. *Eur J Pharm Biopharm*. 2009;71(2):161–172.
14. Jenning V, Gohla SH. Encapsulation of retinoids in solid lipid nanoparticles (SLN). *J Microencapsul*. 2001;18(2):149–158.
15. Lim SJ, Kim CK. Formulation parameters determining the physicochemical characteristics of solid lipid nanoparticles loaded with all-trans retinoic acid. *Int J Pharm*. 2002;243(1–2):135–146.
16. Hu L, Tang X, Cui F. Solid lipid nanoparticles (SLNs) to improve oral bioavailability of poorly soluble drugs. *J Pharm Pharmacol*. 2004;56(12):1527–1535.
17. Kayali I, Ward AJ, Suhery T, Friberg SE, Simion A, Rhein LD. Interactions of retinoic acid with a model of stratum corneum lipids. *J Dermatol Clin Eval Soc*. 1991;2:7–17.
18. Castro GA, Orefice RL, Vilela JM, Andrade MS, Ferreira LA. Development of a new solid lipid nanoparticle formulation containing retinoic acid for topical treatment of acne. *J Microencapsul*. 2007;24(5):395–407.
19. Castro GA, Coelho AL, Oliveira CA, Mahecha GA, Orefice RL, Ferreira LA. Formation of ion pairing as an alternative to improve encapsulation and stability and to reduce skin irritation of retinoic acid loaded in solid lipid nanoparticles. *Int J Pharm*. 2009;381(1):77–83.
20. Souza-Fagundes EM, Queiroz AB, Martins Filho OA, et al. Screening and fractionation of plant extracts with antiproliferative activity on human peripheral blood mononuclear cells. *Mem Inst Oswaldo Cruz*. 2002;97(8):1207–1212.
21. Mosmann T. Rapid colorimetric assay for cellular growth and survival: application to proliferation and cytotoxicity assays. *J Immunol Methods*. 1983;65(1–2):55–63.
22. Riccardi C, Nicoletti I. Analysis of apoptosis by propidium iodide staining and flow cytometry. *Nat Protoc*. 2006;1(3):1458–1461.
23. Munster U, Nakamura C, Haberland A, et al. RU 58841-myristate – prodrug development for topical treatment of acne and androgenetic alopecia. *Pharmazie*. 2005;60(1):8–12.
24. Schafer-Korting M, Mehnert W, Korting HC. Lipid nanoparticles for improved topical application of drugs for skin diseases. *Adv Drug Deliv Rev*. 2007;59(6):427–443.
25. Fanjul AN, Bouterfa H, Dawson M, Pfahl M. Potential role for retinoic acid receptor-gamma in the inhibition of breast cancer cells by selective retinoids and interferons. *Cancer Res*. 1996;56(7):1571–1577.
26. Hong TK, Lee-Kim YC. Effects of retinoic acid isomers on apoptosis and enzymatic antioxidant system in human breast cancer cells. *Nutr Res Pract*. 2009;3(2):77–83.
27. Roberts WR, Addy M. Comparison of the in vivo and in vitro antibacterial properties of antiseptic mouthrinses containing chlorhexidine, alexidine, cetyl pyridinium chloride and hexetidine. Relevance to mode of action. *J Clin Periodontol*. 1981;8(4):295–310.
28. Lappalainen K, Jaaskelainen I, Syrjanen K, Urtti A, Syrjanen S. Comparison of cell proliferation and toxicity assays using two cationic liposomes. *Pharm Res*. 1994;11(8):1127–1131.
29. Scholer N, Olbrich C, Tabatt K, Muller RH, Hahn H, Liesenfeld O. Surfactant, but not the size of solid lipid nanoparticles (SLN) influences viability and cytokine production of macrophages. *Int J Pharm*. 2001;221(1–2):57–67.
30. Zhu WY, Jones CS, Kiss A, Matsukuma K, Amin S, De Luca LM. Retinoic acid inhibition of cell cycle progression in MCF-7 human breast cancer cells. *Exp Cell Res*. 1997;234(2):293–299.
31. Mangiarotti R, Danova M, Alberici R, Pellicciari C. All-trans retinoic acid (ATRA)-induced apoptosis is preceded by G1 arrest in human MCF-7 breast cancer cells. *Br J Cancer*. 1998;77(2):186–191.
32. Hwang SR, Lim SJ, Park JS, Kim CK. Phospholipid-based microemulsion formulation of all-trans-retinoic acid for parenteral administration. *Int J Pharm*. 2004;276(1–2):175–183.

33. Su J, Zhang N, Ho PC. Evaluation of the pharmacokinetics of all-trans-retinoic acid (ATRA) in Wistar rats after intravenous administration of ATRA loaded into tributyrin submicron emulsion and its cellular activity on caco-2 and HepG2 cell lines. *J Pharm Sci*. 2008;97(7):2844–2853.
34. Chen ZX, Breitman TR. Tributyrin: a prodrug of butyric acid for potential clinical application in differentiation therapy. *Cancer Res*. 1994;54(13):3494–3499.
35. Giermasz A, Nowis D, Jalili A, et al. Antitumor activity of tributyrin in murine melanoma model. *Cancer Lett*. 2001;164(2):143–148.
36. Lengsfeld CS, Pitera D, Manning M, Randolph TW. Dissolution and partitioning behavior of hydrophobic ion-paired compounds. *Pharm Res*. 2002;19(10):1572–1576.
37. Martins S, Costa-Lima S, Carneiro T, Cordeiro-da-Silva A, Souto EB, Ferreira DC. Solid lipid nanoparticles as intracellular drug transporters: an investigation of the uptake mechanism and pathway. *Int J Pharm*. 2012;430(1–2):216–227.
38. Serpe L, Catalano MG, Cavalli R, et al. Cytotoxicity of anticancer drugs incorporated in solid lipid nanoparticles on HT-29 colorectal cancer cell line. *Eur J Pharm Biopharm*. 2004;58(3):673–680.
39. Altucci L, Leibowitz MD, Ogilvie KM, de Lera AR, Gronemeyer H. RAR and RXR modulation in cancer and metabolic disease. *Nat Rev Drug Discov*. 2007;6(10):793–810.
40. Bonet ML, Ribot J, Palou A. Lipid metabolism in mammalian tissues and its control by retinoic acid. *Biochim Biophys Acta*. 2012;1821(1):177–189.

# Nanostructured lipid carriers loaded with tributyrin as an alternative to improve anticancer activity of all-trans retinoic acid

**Article** *in* Expert Review of Anti-infective Therapy · February 2015

DOI: 10.1586/14737140.2015.1000868 · Source: PubMed

CITATIONS
13

READS
96

**8 authors**, including:

Elton Luiz Silva
Federal University of Minas Gerais
**5** PUBLICATIONS **74** CITATIONS
SEE PROFILE

Guilherme Carneiro
Universidade Federal dos Vales do Jequitinhonha e Mucuri
**23** PUBLICATIONS **251** CITATIONS
SEE PROFILE

Gisele Castro Goulart
Federal University of Minas Gerais
**5** PUBLICATIONS **59** CITATIONS
SEE PROFILE

Daniel Ferreira Costa
Massachusetts Institute of Technology
**16** PUBLICATIONS **169** CITATIONS
SEE PROFILE

EXPERT REVIEWS

# Nanostructured lipid carriers loaded with tributyrin as an alternative to improve anticancer activity of *all-trans* retinoic acid

*Expert Rev. Anticancer Ther.* 15(2), 247–256 (2015)

Elton Luiz Silva[1], Guilherme Carneiro[2], Priscila Albuquerque Caetano[1], Gisele Goulart[1], Daniel Ferreira Costa[1], Elaine Maria de Souza-Fagundes[3], Dawidson Assis Gomes[4] and Lucas Antônio Miranda Ferreira*[1]

[1]*Department of Pharmaceutics, Faculty of Pharmacy, Universidade Federal de Minas Gerais, Minas Gerais, Brazil*
[2]*Department of Pharmacy, Faculty of Biological and Health Sciences, Universidade Federal dos Vales do Jequitinhonha e Mucuri, Jequitinhonha, Brazil*
[3]*Department of Physiology and Biophysics, Institute of Biological Sciences, Universidade Federal de Minas Gerais, Minas Gerais, Brazil*
[4]*Department of Biochemistry and Immunology, Institute of Biological Sciences, Universidade Federal de Minas Gerais, Belo Horizonte, Brazil*
**Author for correspondence:*
*Tel.: +55 313 409 6939*
*Fax: +55 313 409 6830*
*lucaufmg@gmail.com*

Objectives: *All-trans* retinoic acid (ATRA) is one of the most successful examples of differentiation agents and histone deacetylase inhibitors, such as tributyrin (TB), are known for their antitumor activity and potentiating action of drugs, such as ATRA. Nanostructured lipid carriers (NLC) represent a promising alternative to the encapsulation of lipophilic drugs such as ATRA. This study aims to develop, characterize and evaluate the cytotoxicity of ATRA–TB-loaded NLC for cancer treatment. Methods: The influence of *in situ* formation of an ion pairing between ATRA and a lipophilic amine (benethamine) on the characteristics of NLC (size, zeta potential, encapsulation efficiency) was evaluated. TB, a butyric acid donor, was used as a component of the lipid matrix. *In vitro* activity on cell viability and distribution of cell cycle phases were evaluated for MCF-7, MDA-MB-231, HL-60 and Jurkat cell lines. Results: The presence of the amine significantly increased the encapsulation efficiency of ATRA in NLC. Inhibition of cell viability by TB–ATRA-loaded NLC was more pronounced than the free drug. Analysis of the distribution of cell cycle phases also showed increased activity for TB–ATRA-loaded NLC, with the clear effect of cell cycle arrest in $G_0/G_1$ phase transition. The presence of TB played an important role in the activity of the formulation. Conclusion: Taken together, these findings suggest that TB–ATRA-loaded NLC represents a promising alternative to intravenous administration of ATRA in cancer treatment.

**Keywords:** *all-trans* retinoic acid • cancer • cytotoxicity. • histone deacetylase inhibitors • nanostructured lipid carriers • tributyrin

The concept of differentiation therapy emerged in the 1970s as a promising and revolutionary approach to the treatment of acute myeloid leukemia. *All-trans* retinoic acid (ATRA) is one of the most successful differentiation agents, being used in the treatment of patients with acute promyelocytic leukemia, a subtype of acute myeloid leukemia [1]. Many studies have shown that ATRA is effective against other types of cancer, such as human multiple myeloma, liver and breast carcinomas. ATRA has also been investigated as a chemopreventive agent in the treatment of oral leukoplakia [2,3].

ATRA exerts its actions after binding to the nuclear receptors, retinoic acid receptors and retinoid X receptors, which regulate a variety of genes involved in cell proliferation and differentiation. Generally, ATRA can block the cell cycle in the $G_1$ phase, causing cell proliferation inhibition and apoptosis [4]. In clinical trials, ATRA has been given to cancer patients by oral administration. However, the bioavailability of oral ATRA has been considered low and quite variable [5]. Moreover, continuous treatment with oral ATRA has been associated with progressive reduction of plasma concentrations, probably due to the induced cytochrome P450-dependent metabolism [6]. Whereas these factors limit the clinical use of oral ATRA, an intravenous formulation could circumvent this problem.

The poor aqueous solubility of ATRA, a hydrophobic drug with an octanol/water



 10.1586/14737140.2015.1000868  ISSN 1473-7140 

partition coefficient log of 4.6, can represent an obstacle for intravenous administration [7]. Lipid nanocarriers such as nanoemulsions, solid lipid nanoparticles (SLN), and, recently, nanostructured lipid carriers (NLC) have been studied as alternatives to enable intravenous administration of ATRA [8–10].

NLC have been developed to circumvent the limitations offered by the polymorphic transitions observed in the lipid matrix of SLN. NLC are prepared from a mixture of liquid and solid lipids that maintain a solid state at the end of preparation [11]. The presence of liquid lipid increases the number of imperfections in the solid lipid matrix, allowing greater accommodation for the drug and decreasing its expulsion over time [12]. In recent years, some studies have been developed using NLC loaded with ATRA for the treatment of cancer [10,13].

Usually, ATRA encapsulation in these nanocarriers is low. We had previously reported that the *in situ* formation of an ion pairing among ATRA, a lipophilic acid, and lipophilic amines provides an interesting alternative to increase drug encapsulation in SLN [14]. Recently, a SLN formulation was developed and evaluated by Carneiro and colleagues [15] using the formation of an ion pairing between ATRA and a lipophilic amine, benethamine (BNT), with potential application for the cancer treatment.

On the other hand, histone deacetylase inhibitors, such as tributyrin (TB), are known for their antitumor activity and potentiating action of other drugs such as ATRA [16,17]. Moreover, the lipophilic nature of TB enables its use as a component of the oily core of nanoemulsions [18] and related nanosystems. In this sense, this study aims to develop a new innovative formulation of NLC loaded with ATRA and TB as an alternative for the treatment of cancer. The influence of *in situ* formation of an ion pairing between ATRA and BNT on the characteristics of NLC was evaluated. Also, *in vitro* anticancer activity was investigated against different cancer cell lines: breast cancer and leukemia cells.

## Materials & methods

### Materials

ATRA and Compritol® 888 ATO (glyceryl behenate, mixture of mono-, di- and triacylglycerols of behenic acid [$C_{22}$]) were kindly provided by BASF (Ludwigshafen, Germany) and Gattefossé (Lyon, France), respectively. Super Refined Tween 80™ (Polysobarte 80) was provided by Croda Inc (Edison, NJ, USA). TB and BNT (*N*-Benzyl-2-phenylethylamine) were purchased from Sigma-Aldrich (St Louis, MO, USA). Hydrogenated soybean lecithin (Lipoid S 75-3) was purchased from Lipoid (Ludwigshafen, Germany). For *in vitro* studies, the Roswell Park Memorial Institute medium 1640 was obtained from Sigma-Aldrich (St Louis, MO, USA); Dulbecco's modified Eagle's medium, fetal bovine serum, 3-(4,5-dimethylthiazol-2-yl)-2,5-diphenyl tetrazolium bromide (MTT), staurosporine and propidium iodide were purchased from Life Technologies (Carlsbad, CA, USA). The following cancer cell lines were used: Jurkat (immortalized line of T lymphocyte) was provided by Gustavo Amarante-Mendes from São Paulo University (São Paulo, SP, Brazil); MCF-7 (human breast adenocarcinoma), MDA-MB-231 (human breast adenocarcinoma, derived from metastatic site) and HL-60 (acute promyelocytic leukemia) cells were purchased from American Type Culture Collection (Manassas, VA, USA). All other chemicals were of analytical grade.

### Preparation of NLC

NLC were prepared by the hot melting homogenization method using an emulsification-ultrasound as previously described [19]. The composition of the formulations was based on previous studies [15], but with some modifications. In brief (batch 10 ml), the oily phase, composed of Compritol 888 ATO (150 mg), TB (50 mg), Tween 80™ (50 mg), Lipoid S 75-3 (50 mg), ATRA (5 mg) and the aqueous phase were heated separately to 85°C. Next, the aqueous phase was gently dropped onto the oily phase with constant agitation at 8000 rpm in an Ultra Turrax T-25 homogenizer (Ika Labortechnik, Staufen, Germany). This emulsion was immediately submitted to the high-intensity probe sonication (20% amplitude) for 10 min, using a high-intensity ultrasonic processor (CPX 500 model; Cole-Parmer Instruments, Vernon Hills, IL, USA). The pH of the NLC was adjusted to 7.0 with a solution of 0.01 M HCl (Digimed DM 20, Campo Grande, MS, Brazil). Considering the intended use of NLC (intravenous administration), Tween 80™ and Lipoid S 75-3 were selected as surfactants. The influence of the *in situ* formation of an ion pairing between ATRA and the lipophilic amine BNT was investigated (ATRA/BNT molar ratio was 1/2).

### Particle size analysis

The mean particle diameter of NLC in the dispersion was determined by unimodal analysis through dynamic light scattering using a Zetasizer Nano-ZS90 (Malvern Instruments, Malvern, UK), at a fixed angle of 90° and 25°C. The NLC dispersions were diluted in distilled and filtered water (cellulose ester membrane, 0.45 µm, Millipore, Billerica, MA, USA). The data reported were particle size, evaluated as the intensity obtained from three repeat measurements, and the polydispersity index.

### Zeta potential

Zeta potential measurements were carried out by the electrophoretic light scattering determination using a Zetasizer Nano-ZS90 (Malvern Instruments, Malvern, UK), at 90° and 25°C. Before the measurements, NLC dispersions were diluted in distilled and filtered water (cellulose ester membrane, 0.45 µm, Millipore, Billerica, MA, USA). All measurements were performed in triplicate.

### Drug-encapsulation efficiency

Encapsulation efficiency (EE) for ATRA in NLC was determined according to the method previously described [19]. This method was based on the determination of ATRA concentration in the NLC (before and after filtration; cellulose ester membrane, 0.45 µm, Millipore, Billerica, MA, USA) as well as in the external aqueous phase of the NLC, which was estimated by ultrafiltration method (Amicon® 100 k, Millipore, Billerica, MA, USA) using a 100 kDa molecular weight cut-off membrane.

In brief, an aliquot of the NLC dispersion was dissolved in tetrahydrofuran and later diluted in a mixture of acetonitrile:distilled water:phosphoric acid (80:19.9:0.1). This mixture keeps the ATRA in solution (dissolved), but causes lipid precipitation. This dispersion was filtered in a 0.45 μm Millex HV filter (Millipore, Billerica, MA, USA) and analyzed by HPLC.

The HPLC system consisted of a Waters 515 HPLC Pump (Milford, MA, USA), a Waters 717 Plus Auto-sampler, and a photodiode array detector (Waters 2996). A C18 reverse-phase column (125 mm of length, 4 mm of width and particles of 5 μm) (LichroCart 125–4, Merck, Darmstadt, Germany) was used. The mobile phase was a mixture of acetonitrile, distilled water and phosphoric acid (80:19.9:0.1). The detection was carried out at 340 nm, with a flow rate of 1.0 ml/min and 20 μl of sample. The five-point (0.25, 0.5, 1.0, 2.0 and 5.0 μg/ml) linear regression analysis resulted in the following linear equation: $y = -2435 + 137200 \times$ ($r = 0.9998$).

Considering that the ATRA concentration found in the aqueous phase was negligible, EE was calculated using the following formula: EE (%) = (filtered ATRA/total ATRA) × 100.

### Polarized light microscopy

The presence of ATRA crystals was evaluated by polarized light microscopy (Zeiss Axio Imager.M2, Carl Zeiss, Oberkochen, Germany). The samples were prepared in microscope slides (undiluted), utilizing a proper software (ZEN lite 2012, Carl Zeiss, Oberkochen, Germany). The microscope was equipped with an AxioCam digital camera (Model ERc 5S, Carl Zeiss, Oberkochen, Germany).

### Transmission electron microscopy

Morphological examination of the NLC was performed with a transmission electron microscope (Tecnai G2-12, Spirit Biotwin, 120 kV, FEI, Hillsboro, OR, USA) using a negative staining method. The sample was prepared by placing a drop of NLC (dilution 1/50 in double-distilled water) onto a copper grid coated with carbon film. The excess droplets were removed with a filter paper. After three washings with water, the samples were stained with 2% (w/v) uranyl acetate in ethanol. The grid was dried at room temperature and then observed by transmission electronic microscopy.

### Differential scanning calorimetry

Differential scanning calorimetry (DSC) analyses were performed using a DSC 2910, (TA Instruments, New Castle, DE, USA). For DSC measurements, a scan rate of 10°C/min was used at a temperature range of 0–250°C, under nitrogen purge (50 ml/min). Lyophilized NLC were obtained using a freeze-drier (E-C Apparatus) connected to an E2M18 vacuum pump (BOC Edwards, UK), after rapid freezing of the NLC preparation into liquid nitrogen. The samples were lyophilized for 24 h at a temperature of −45°C. After freeze-drying, the lyophilized samples were placed directly in aluminum pans for DSC analyses. The ion pairing ATRA–BNT was prepared separately according to the following protocol: in brief, ATRA and BNT (molar ratio 1:1) were solubilized with a freshly prepared solution of methanol and chloroform (1:1). The reactional mixture was kept under agitation for 6 h at room temperature and protected from light exposure. Then, solvents were evaporated in a rotary evaporator (R-215, Büchi, Flawil, Switzerland) utilizing a vacuum pump (V-700, Büchi, Flawil, Switzerland) and heating bath (B-491, Büchi, Flawil, Switzerland) at 45°C. The residue was collected and stored at −20°C before analysis.

### Cell cultures

Cancer cell lines MCF-7 (human mammary adenocarcinoma), MDA-MB-231 (human mammary adenocarcinoma), HL-60 (human acute promyelocytic leukemia) and Jurkat (human acute T cell leukemia) were cultured in Dulbecco's modified Eagle's medium or Roswell Park Memorial Institute medium containing fetal bovine serum (10%), 200 mM glutamine, and antibiotics (100 μg/ml streptomycin and 100 UI/ml penicillin). All cultures were kept in a humidified incubator with 5% $CO_2$ at 37°C.

### Analysis of cell viability

Cell proliferation was measured by MTT assay based on the reduction of tetrazolium salt to formazan crystals by living cells. In brief, aliquots containing $7.0 \times 10^3$ (MCF-7), $2.5 \times 10^3$ (MDA-MB-231), $9 \times 10^3$ (HL60) or $1.8 \times 10^4$ (Jurkat) cells/well were seeded into 96-well plates. After 24 h of incubation at 37°C and 5% $CO_2$, freshly prepared solutions of free ATRA and ATRA-loaded NLC were added to the wells (ATRA concentration ranged from 0.5 to 50 μM). Free ATRA was dissolved in dimethyl sulfoxide (DMSO) (33.3 mM) before dilution. Blank NLC (without ATRA) was diluted in the same way as ATRA-loaded NLC to simulate the same range of ATRA concentration. After 48 h of incubation at 37°C and 5% $CO_2$, 20 μl of the 5 mg/ml MTT solution was added to each plate. Plates were incubated at 37°C for 4 h, and then the medium was replaced by 200 μl of 0.04 M HCl solution in isopropanol. Cell viability was estimated by measuring the rate of mitochondrial reduction of MTT, determined by evaluating the absorbance of the converted dye at a wavelength of 595 nm. Absorbance values of the wells in which the cells were maintained in medium alone were considered as 100% of cell viability. Control groups included treatment with DMSO (negative control) and staurosporine (positive control). Cell viability was found to be 100% after treatment with negative control (DMSO 0.5%), whereas staurosporine was effective in promoting cell growth inhibition. Data were expressed as percentage of cell viability compared with the control (mean ± standard deviation). At least three independent experiments were performed.

### Subdiploid DNA content & cell cycle analysis

A flow-cytometric DNA fragmentation assay was employed as a quantitative measure of subdiploid content and phases of the cell cycle [20]. Aliquots containing $5.0 \times 10^4$ (MCF-7, MDA-MB-231 and HL-60) or $1.0 \times 10^4$ cells/well (Jurkat) were seeded into 24-well plates and incubated for 24 h at 37°C and 5% $CO_2$. After incubation, cells were treated with free ATRA,

**Table 1. Characterization of blank nanostructured lipid carriers and *all-trans* retinoic acid-loaded nanostructured lipid carriers (A and B) for particle diameter, polydispersity index and zeta potential.**

| Parameter | Blank NLC | ATRA-loaded NLC | |
|---|---|---|---|
| | | *NLC-A 0% BNT* | *NLC-B 0,1% BNT* |
| Mean diameter (nm) | 131 ± 4[†] | 171 ± 18[‡] | 154 ± 4 |
| Polydispersity index | 0.25 ± 0.03 | 0.40 ± 0.11[‡] | 0.24 ± 0.03 |
| Zeta potential (mV) | −38 ± 4 | −33 ± 5 | −43 ± 7 |

Data are shown as mean ± SD (n = 3).
[†]Significant difference compared with NLC-A and NLC-B ($p < 0.05$);
[‡]Significant difference compared with blank NLC and NLC-B ($p < 0.05$).
ATRA: *All-trans* retinoic acid; BNT: Benethamine; NLC: Nanostructured lipid carrier.

ATRA-loaded NLC or blank NLC for 48 h at 37°C and 5% $CO_2$ (ATRA concentration was 25 µM). After this time, cells were centrifuged at 200 g for 5 min at room temperature, and the culture medium was aspirated off. The pellet was gently resuspended in 300 µl of hypotonic fluorochrome solution containing 0.5% Triton X-100 and 50 µg/ml propidium iodide. Cells were incubated in the dark at 4°C for 4 h and analyzed with a Guava® EasyCyte™ 6-2L Base System cytometer (Millipore, Billerica, MA, USA). Data analysis was performed with FlowJo™ 7.6.5 (Tree Star Inc, Ashland, OR, USA) to determine percentages of subdiploid content and phases of the cell cycle.

### *Data analysis*

Statistical analyses were carried out using one-way analysis of variance followed by Tukey's test. For all analyses, the difference was considered statistically significant when p value was less than 0.05.

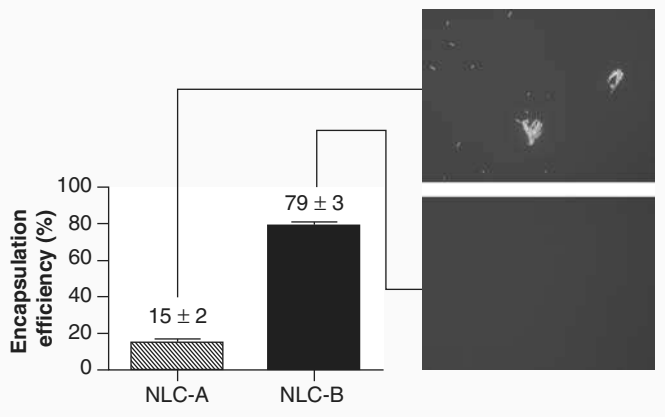


**Figure 1. Encapsulation efficiency of a*ll-trans* retinoic acid-loaded nanostructured lipid carriers formulations in absence (NLC-A) and presence (NLC-B) of the lipophilic amine benethamine.** Data are shown as mean ± SD, n = 3. ATRA crystals can be clearly observed in the external phase of NLC without BNT (polarized light microscopy images, 200 × magnification).
ATRA: A*ll-trans* retinoic acid; BNT: Benethamine; NLC: Nanostructured lipid carriers; SD: Standard deviation.

## Results

### *Characterization of NLC*

The main characteristics of blank NLC and ATRA-loaded NLC prepared with lipophilic amine BNT are listed in Table 1. The addition of ATRA (NLC A, 171 ± 18 nm) and ATRA + BNT ion pairing (NLC-B, 154 ± 4) increased the mean particle size in comparison to blank NLC (131 ± 4 nm). Mean particle sizes and polydispersity index for NLC A (171 ± 18 nm and 0.40 ± 0.11, respectively) were higher than those observed for NLC-B (154 ± 4 nm and 0.24 ± 0.03). This increase is directly related with ATRA crystals present in its external aqueous phase of NLC-A (Figure 1).

Negatively charged particles were obtained for blank NLC (−38 ± 4 mV) and ATRA-loaded NLC (NLC-A: −33 ± 5 mV, and NLC-B: −43 ± 7 mV). The presence of BNT did not change the surface charge of NLC (compare NLC-A and NLC-B). This can be attributed to its low potential for interfacial adsorption [15].

The EE for ATRA in NLC without BNT increased from 15 ± 2% (NLC-A) to 79 ± 3% for NLC with BNT (NLC-B) (Figure 1). Therefore, BNT promoted a significant increase of EE for ATRA in NLC prepared with TB as a component of the lipid matrix. This increase in the EE could be due to the formation of an ion pairing between ATRA and BNT, which increases the lipophilic properties of the drug, making its incorporation into the lipid matrix easier (Figure 1). The presence of ATRA crystals was investigated in the NLC presenting low EE (without BNT) and high EE (with BNT) (insert Figure 1). ATRA crystals were clearly present in the external phase of NLC without BNT. However, these crystals were absent in NLC with BNT (NLC-B). These findings are in agreement with our previous observations that showed the role of the lipophilic amines (stearylamine and BNT) in increasing ATRA drug-loading capacity in SLN [15,19].

### *Transmission electronic microscopy*

The NLC image obtained by transmission electronic microscopy is shown in Figure 2. Blank NLC had nearly spherical shapes with little variability in shape and size (~100 nm). The values of particle sizes were lower than those determined by dynamic light scattering. In fact, dynamic light scattering measures the hydrodynamic diameter of the particles and this could explain these differences.

### *Differential scanning calorimetry*

The data of DSC analyses are shown in Figure 3. Compritol 888 ATO, ATRA, and the ATRA+BNT ion pairing presented the following endothermic melting point peaks: 75°, 187° and 114°C, respectively (Figure 3A). The melting point peak for the ion pairing was lower than that observed for the pure drug and this suggests that a different crystalline structure was formed from pure ATRA. The melting points for ATRA and the ion pairing were absent in the ATRA-loaded NLC (Figure 3B) and only the Compritol 888 ATO peak is shown, suggesting that ATRA is integrated in the lipid. On the other hand, it was also

possible to note a slight decrease in the melting point of the lipid matrix for the ATRA-loaded NLC in comparison to blank NLC (from 76° to 74°C), as well as a gradual broadening of this peak (Figure 3B). These modifications can be attributed to the incorporation of the ion pairing (ATRA+BNT) in the lipid matrix of the NLC.

### *Cell viability studies*

MTT assay was used to evaluate whether cytotoxicity of ATRA was affected by loading in NLC. Cancer cell lines MCF-7, MDA-MB-231, HL-60 and Jurkat were incubated with free ATRA, blank NLC (unloaded) or ATRA-loaded NLC and analyzed for their viability. The data obtained, expressed as cell viability (percentage), are shown in Figure 4.

For MCF-7 cells, blank NLC showed no inhibitory activity up to an ATRA concentration of 10 μM. Thereafter, a reduction in cell viability to about 80% at the highest concentration was observed. This activity can be attributed to the TB, present in the NLC matrix, which can act as a butyric acid donor, causing the observed reduction in cell viability. In fact, an NLC containing caprylic/capric triglycerides as liquid lipid instead of TB was evaluated and this formulation had no effect on the cell viability (data not shown). The activity of free ATRA was low regardless of the concentration with cell viability of around 80%. The cytotoxicity of ATRA-loaded NLC was significantly higher than that observed for the free RA and blank NLC, reducing the cell viability to approximately 60% at 50 μM.

Leukemic cells (HL-60 and Jurkat) were more sensitive to ATRA, whereas the MDA-MB-231 cells were the least sensitive. In fact, free ATRA showed negligible cytotoxic effect in MDA-MB-231 cells at all evaluated concentrations. In contrast, cytotoxic activity for ATRA-loaded NLC was significantly higher than that observed for free ATRA. Unexpectedly, however, differences between ATRA-loaded NLC and blank NLC were negligible. Taken together, these data suggest that activity observed for NLC with or without ATRA could be attributed to the release of butyric acid from TB, which was added into lipid matrix of the NLC.

For HL-60 cells, the activity for free ATRA and ATRA-loaded NLC was dose-dependent with the formulation showing cytotoxicity higher than that observed for free ATRA mainly at lower drug concentrations. For example, the cell viability at 0.5 μM was 60 ± 8% and 80 ± 4% for ATRA-loaded NLC and free ATRA, respectively. For Jurkat cells, cell viability after

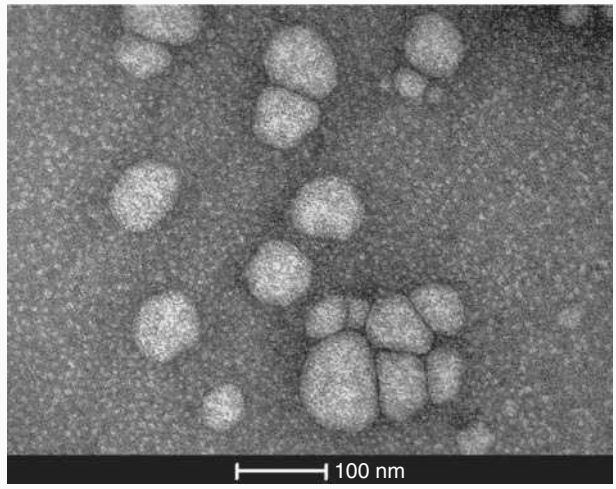


**Figure 2. Transmission electron microscopy images of blank nanostructured lipid carriers.** The particles were fixed with solution of uranyl acetate at 2% and dried at room temperature prior to imaging. Transmission electron microscopy analysis were performed with blank nanostructured lipid carriers in order to avoid any effect on the picture quality due to the precipitation of non-encapsulated a*ll-trans* retinoic acid crystals during the sample preparation.

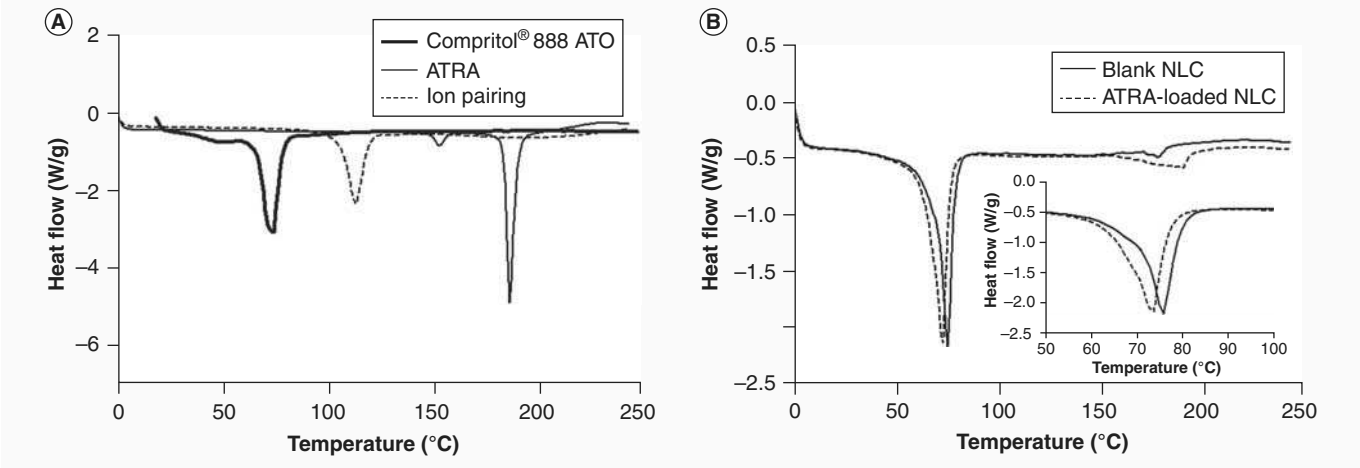


**Figure 3. Differential scanning calorimetry thermograms of nanostructured lipid carriers. (A)** Main ingredients (Compritol® 888 ATO, ATRA and ion pairing ATRA-BNT – thermogram) and **(B)** NLC formulations (Blank NLC and ATRA-loaded NLC – thermogram). ATRA: A*ll-trans* retinoic acid; BNT: Benethamine; NLC: Nanostructured lipid carriers.

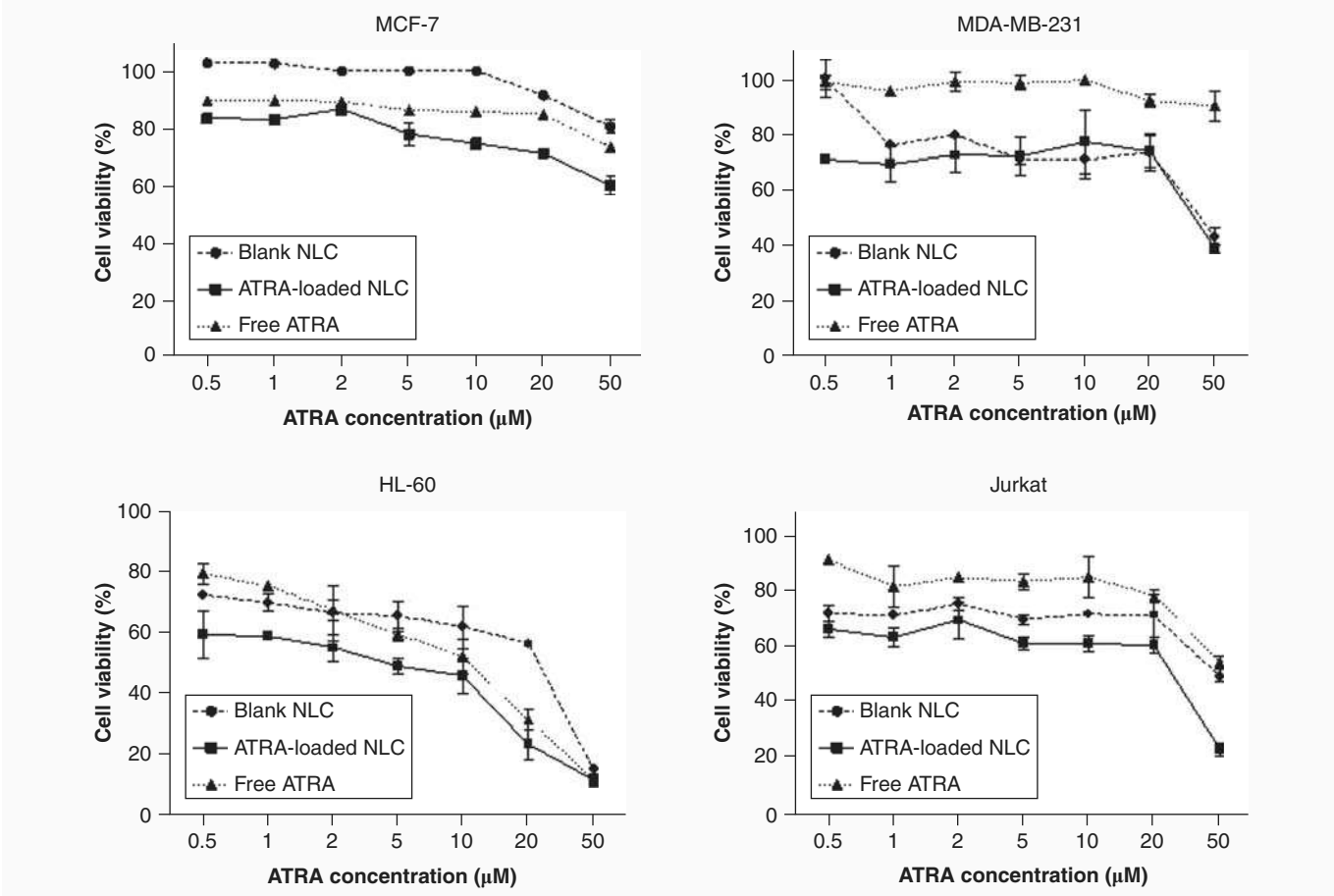


**Figure 4. Cell viability studies, as evaluated by MTT assay, of blank NLC, ATRA-loaded NLC and free ATRA in cancer cells, MCF-7, MDA-MB-231, HL-60 and Jurkat, after 48 h of exposure.**
Data were expressed as mean ± SD of three independent experiments. The blank NLC were diluted at the same proportion as ATRA-loaded NLC.
ATRA: *All-trans* retinoic acid; BNT: Benethamine; MTT: 3-(4,5-dimethylthiazol-2-yl)-2,5-diphenyl tetrazolium bromide; NLC: Nanostructured lipid carriers.



treatment with free ATRA was around 80% at most concentrations tested, with higher activity at 50 μM (54 ± 2%). For blank NLC, cell viabilities were around 70% and a greater effect was observed at 50 μM (50 ± 2%). The activity for ATRA-loaded NLC was significantly higher than that observed for free ATRA and blank NLC with a much greater effect at 50 μM (23 ± 2%). The cytotoxic activity of ATRA-loaded NLC was clearly improved in comparison to free ATRA and this was attributed to the butyric acid released by hydrolysis of TB.

### *Subdiploid DNA content & cell cycle analysis*

Flow cytometry studies were performed to determine whether the improvement of the cytotoxic activity of ATRA after incorporation into NLC was associated with alterations in DNA fragmentation and/or distribution of the cell cycle phase. The data are summarized in Table 2. Representative histograms of cell cycle distribution after cell staining with propidium iodide are shown in Figure 5.

The increase in subdiploid DNA content for all treatments (blank NLC, free ATRA, and ATRA-loaded NLC) was negligible in comparison to control as its value was less than 1% for all cell lines evaluated (Table 2). Nevertheless, the effects of ATRA encapsulation in NLC became more evident when analyzing the distribution of cell cycle phases. For MCF-7 cells, the percentage of cells in the $G_0/G_1$ phase for ATRA-loaded NLC (84.9 ± 0.6%) was increased ($p < 0.05$) when compared with control and free ATRA (70.9 ± 3.8% and 77.7 ± 1.8%, respectively). Moreover, the increase in the $G_0/G_1$ phase was followed by a significant decrease in the percentage of cells in the S and $G_2/M$ phases, as shown in Table 2 and illustrated in Figure 5. The effect of blank NLC was similar to that observed for free ATRA, with a significant increase ($p < 0.05$) in the number of cells in $G_0/G_1$ compared with control. As suggested for the MTT assay, the effect of this formulation can be attributed to the presence of TB.

For MDA-MB-231 cells, it was observed that free ATRA did not arrest the cells in $G_0/G_1$. In contrast, blank NLC

caused a significant increase of cells in $G_0/G_1$ (76.3 ± 0.7%) compared with control (70.7 ± 1.3%) and free ATRA (60.1 ± 1.2%). The effect of ATRA-loaded NLC (85.7 ± 1.2%) was even more pronounced than that observed for blank NLC. In agreement, the decrease in the S phase for ATRA-loaded NLC (4.5 ± 0.3%) was also significantly higher than that observed for blank NLC (9.4 ± 1.3%) and this suggests cell cycle arrest in $G_0/G_1$, as occurred for MCF-7 cells.

The most intense effect of cell cycle arrest in $G_0/G_1$ was observed for HL-60 cells. Free ATRA had a significant effect (94.5 ± 0.8%) compared with control (77.5 ± 1.1%). Blank NLC also caused an increase in $G_0/G_1$ (82.7 ± 2.3%), but lower than that observed for free ATRA. For ATRA-loaded NLC, almost 99% of the cells were in the $G_0/G_1$ phase. These data are in agreement with those observed in the MTT assay, which, in concentration of 20 μM (close to that used in flow cytometry), ATRA-loaded NLC and free ATRA caused important reduction in cell viability. The decrease in the S and $G_2/M$ phases for ATRA-loaded NLC was statistically significant compared with the control. Free ATRA also showed a significant decrease in the S phase (2.9 ± 1.2%), which was revealed to be lower than that observed for the treatment with ATRA-loaded NLC (0.4 ± 0.1%).

For Jurkat cells, free ATRA had no significant differences in comparison to control for any of the cell cycle phases. Blank NLC showed a small but significant increase in the percentages of cells in $G_0/G_1$ compared with control. The ATRA-loaded NLC provided a significant increase in $G_0/G_1$-phases in comparison to the control and free ATRA.

**Table 2. Effects of different treatments on DNA fragmentation and cell-cycle phases distribution of the breast cancer (MCF-7 and MDA-MB-231) and leukemic cell lines (HL-60 and Jurkat).**

| Sample | Cell cycle distribution (%) | | | |
|---|---|---|---|---|
| | *Subdiploid* | *$G_0/G_1$* | *S* | *$G_2/M$* |
| | | ***MCF-7*** | | |
| Control | NS† | 70.9 ± 3.8 | 10.9 ± 0.4 | 17.8 ± 3.6 |
| Free ATRA | NS | 77.7 ± 1.8 | 6.96 ± 0.5 | 15.3 ± 1.3 |
| Blank NLC | NS | 80.9 ± 0.5 | 6.6 ± 0.1 | 12.5 ± 0.4 |
| ATRA-loaded NLC | NS | 84.9 ± 0.6‡ | 4.6 ± 0.2 | 10.0 ± 1.0 |
| | | ***MDA-MB-231*** | | |
| Control | NS | 70.7 ± 1.3 | 12.0 ± 0.1 | 17.2 ± 1.5 |
| Free ATRA | NS | 60.1 ± 1.2 | 12.1 ± 0.2 | 27.5 ± 0.9 |
| Blank NLC | NS | 76.3 ± 0.7 | 9.4 ± 1.3 | 13.9 ± 0.6 |
| ATRA-loaded NLC | NS | 85.7 ± 1.2§ | 4.5 ± 0.3 | 9.5 ± 1.1 |
| | | ***HL-60*** | | |
| Control | NS† | 77.5 ± 1.1 | 9.8 ± 2.5 | 12.5 ± 1.3 |
| Free ATRA | NS | 94.5 ± 0.8 | 2.9 ± 1.2 | 2.6 ± 0.4 |
| Blank NLC | NS | 82.7 ± 2.3 | 7.3 ± 1.1 | 10.1 ± 1.2 |
| ATRA-loaded NLC | NS | 98.5 ± 0.1§ | 0.4 ± 0.1 | 1.2 ± 0.1 |
| | | ***Jurkat*** | | |
| Control | NS | 60.7 ± 8.5 | 20.2 ± 4.9 | 19.1 ± 3.5 |
| Free ATRA | NS | 65.7 ± 2.3 | 17.6 ± 1.2 | 16.8 ± 1.0 |
| Blank NLC | NS | 73.0 ± 0.3 | 12.4 ± 0.8 | 14.6 ± 0.6 |
| ATRA-loaded NLC | NS | 78.6 ± 2.5‡ | 11.0 ± 0.9 | 10.5 ± 1.6 |

Cancer cells were treated with ATRA-loaded NLC, free ATRA and unloaded (blank) NLC, as indicated in the methods section. Cell-cycle distributions were determined after 48 h of treatment. The data are representative of three independent experiments. Mean ± SD is shown.
†Non-significant (less than 1.0%).
‡Significant difference compared with control and free ATRA ($p < 0.05$).
§Significant difference compared with control, free ATRA and blank NLC ($p < 0.05$).
ATRA: *All-trans* retinoic acid; NLC: Nanostructured lipid carriers; SD: Standard deviation.

## Discussion

The aim of this study was to develop and evaluate the *in vitro* cytotoxic activity of NLC loaded with ATRA and TB. The EE for ATRA in NLC was significantly increased after the addition of the lipophilic BNT (from 15 ± 2% to 79 ± 3 %, Figure 1). Therefore, BNT promoted a significant increase of EE for ATRA in NLC. These findings are consistent with our previous observations [15,19]. In agreement, the data of DSC revealed the absence of melting point peaks for ATRA and ion pairing in ATRA-loaded NLC, suggesting that ATRA was integrated in the lipid. The ion pairing-induced modifications in the lipid matrix of the ATRA-loaded NLC suggest a larger number of defects, allowing greater encapsulation for the ATRA in NLC.

Cytotoxic effects against four important tumor cell lines were evaluated. With respect to cell viability studies, a clear advantage was observed when ATRA-loaded NLC was compared with free ATRA and blank NLC for the MCF-7 line. The results obtained for free ATRA in MCF-7 cells were comparable with findings previously described [15,21]. The accumulation of MCF-7 cells in $G_0/G_1$ for ATRA-loaded NLC was accompanied by a reduction in the frequency of cells in the S and $G_2/M$ phases. These findings are consistent with previous observations, which showed that treatment of MCF-7 cells with ATRA induces cell cycle arrest in $G_0/G_1$ before inducing apoptosis [22,23].

Remarkably, for MDA-MB-231 cells, it was suggested that the activity of ATRA-loaded NLC and blank NLC results from

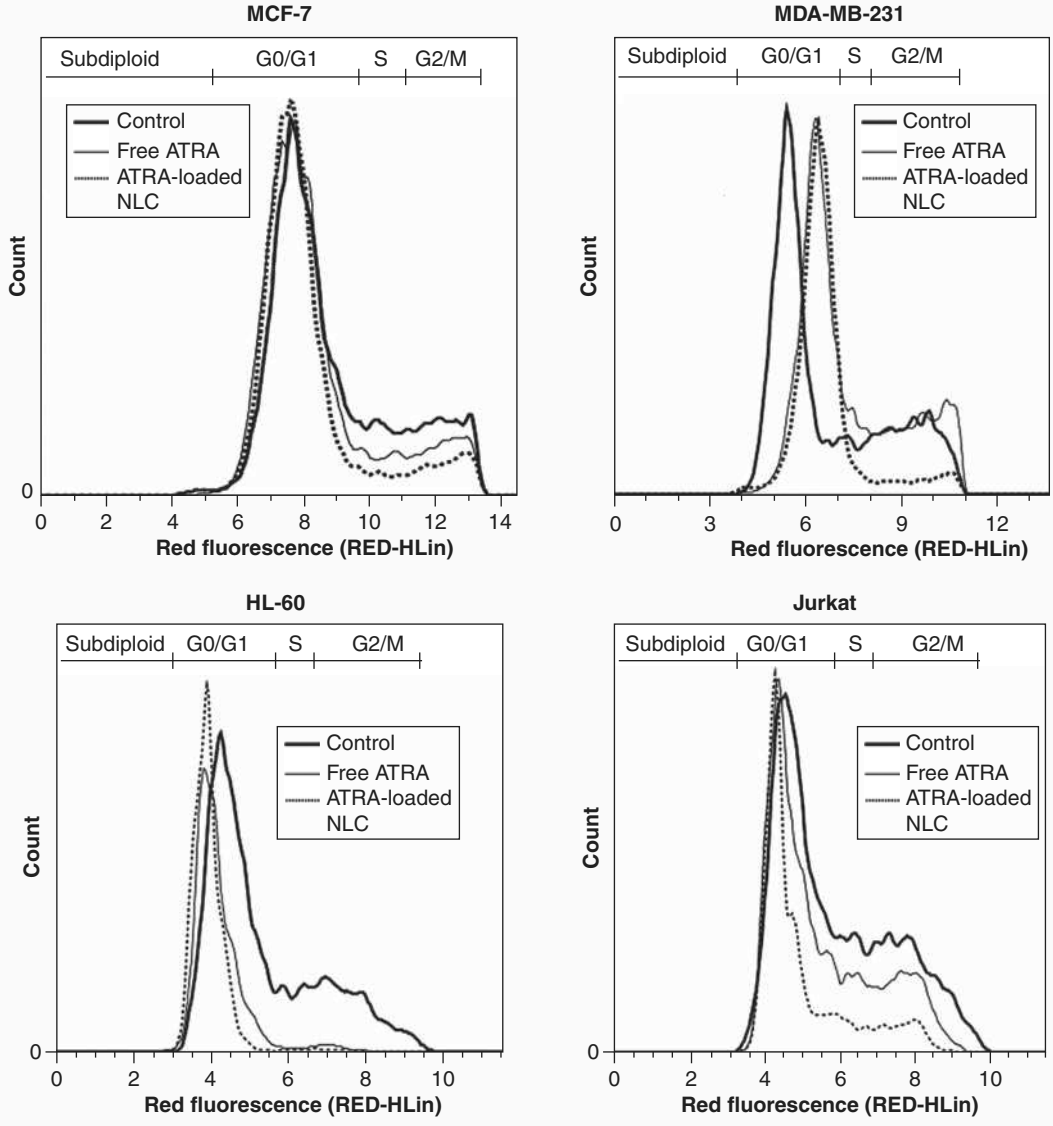


**Figure 5. Illustrative DNA fluorescence histograms of PI-stained MCF-7, MDA-MB-231, HL-60 and Jurkat cells after 48 h of incubation comparing the effect of free a*ll-trans* retinoic acid and a*ll-trans* retinoic acid encapsulated in nanostructured lipid carriers with the control treatment (medium alone).**

ATRA was used at 25 μM. ATRA-loaded NLC induced cell-cycle arrest accompanied by reduction in the S and G2/M phases in the cells. Data from one representative experiment that represents 20,000 events (cells) are shown.

ATRA: *All-trans* retinoic acid; NLC: Nanostructured lipid carriers; PI: Propidium iodide.

the release of butyric acid from TB hydrolysis. In fact, free ATRA showed negligible activity against MDA-MB-231 cells confirming the intrinsic resistance of these cells to ATRA. Estrogen-independent cell lines, such as MDA-MB-231, are known for their low expression of RA receptors α, which justifies its resistance to the effects of ATRA [24]. Evaluating the data of distribution of cell cycle phases presented in Table 2 clearly showed that ATRA-loaded NLC had the most pronounced effect in promoting cell cycle arrest in $G_0/G_1$. The differences between blank NLC and ATRA-loaded NLC in the MTT assay were insignificant and this can be related to the lower sensitivity of this technique compared with flow cytometry. On the other hand, profiles in Figure 5 for MDA-MB-231 cells treated with free ATRA or loaded in NLC revealed a peak shift in comparison with the control group and this can be attributed to some degree of aneuploidy (DNA content different from 2n). Aneuploidy has been described by several authors and is a common finding in tumor cells and other organisms, being characterized by irregular number of chromosomes [25]. As described by Cappello *et al.* 2014 [26], aneuploid MDA-MB-231 cells were identified in flow cytometry analysis with fluorescence intensity higher than diploid cells ($G_0/G_1$) but lower than $G_2/M$ cells. This phenomenon was also observed for pluripotent stem cells undergoing differentiation induced by ATRA [27].

An ATRA-sensitive (HL-60) and an ATRA-resistant leukemic cell line (Jurkat) were evaluated in this study. ATRA-loaded NLC showed a significant accumulation in the $G_0/G_1$ phase when compared with free ATRA and the control for both cells, with a more pronounced effect in Jurkat cells. These data are in agreement with those obtained in studies of cell viability. ATRA resistance has been related to various events, including increased catabolism and genetic alterations [28]. The protection against increased metabolism may represent one of the advantages offered by ATRA encapsulation in NLC. In Jurkat cells, ATRA resistance is associated with the negativity of human T cell leukemia virus Type 1 [29]. The differences between ATRA-loaded NLC and blank NLC were not significant in Jurkat cells, suggesting that the presence of TB, as a butyric acid donor, had an essential role in the activity of this formulation. These findings are in agreement with those previously published showing significant cytotoxic activity of butyric acid against Jurkat cells [30]. Taken together, the data suggest that ATRA-loaded NLC represent a novel approach that is potentially significant in the field of ATRA resistance.

It is noteworthy that for all cell lines evaluated, none of the treatments induced significant cell death, with values of subdiploid DNA content less than 1%. These findings are not unexpected, as several studies have shown that one of the main activities of ATRA is the cell cycle arrest in the $G_0/G_1$ phase, followed by differentiation and/or apoptosis [31]. In leukemic cells, for example, it is well known that treatment with inducers of differentiation, such as ATRA, makes the cells become resistant to apoptosis during the early stages of differentiation. Apoptosis occurs in such cases as a later event constituting an alternative fate for cells that for some reason are not able to resume the normal differentiation program [32].

Finally, TB as an oily core of a nanoemulsion provided the dual function of solubilizing the celecoxib and potentiating its cytotoxic activity [18]. In addition, the cytotoxicity of ATRA-loaded TB nanoemulsion against hepatic or colonic cancer cells was higher than that of free ATRA [17]. However, in this study, it is difficult to separate the effects of the combination of ATRA and TB from those of drug encapsulation, and data concerning drug encapsulation and comparison with blank nanoemulsion were not reported. In this study, we reported for the first time a remarkable increase in anticancer activity of ATRA–TB-loaded NLC in comparison with free ATRA against leukemic cells using a formulation with high drug encapsulation.

## Conclusion

In summary, an NLC formulation loaded with ATRA, a lipophilic acid, and a lipophilic amine (BNT) was designed and evaluated. It was possible to obtain high EE for ATRA in NLC. Moreover, ATRA-loaded NLC promoted enhanced *in vitro* cytotoxic activity when compared with the free ATRA. TB, present in the lipid matrix of NLC, played an important role in the activity of the formulation. These findings suggest that the ATRA-loaded NLC is a promising alternative for the administration of ATRA in the treatment of cancer.

### Acknowledgements

*The authors wish to thank G Hawes, M.Ed. English Education, University of Georgia, USA, for editing this manuscript.*

### Financial & competing interests disclosure

*This study was supported by NIH Grant 1R03TW008709 and by grants from Minas Gerais State Agency for Research and Development (FAPEMIG, Brazil) and by the Brazilian agencies CAPES and CNPq. The authors have no other relevant affiliations or financial involvement with any organization or entity with a financial interest in or financial conflict with the subject matter or materials discussed in the manuscript apart from those disclosed.*

*No writing assistance was utilized in the production of this manuscript.*

## Key issues

- This study aimed to develop and evaluate the *in vitro* cytotoxic activity of nanostructured lipid carriers (NLC) loaded with *all-trans* retinoic acid (ATRA) and tributyrin (TB). TB is a histone deacetylase inhibitor known for its antitumor activity and potentiating action of drugs such as ATRA.
- The lipophilic amine BNT promoted a significant increase of encapsulation for ATRA in NLC.
- Cytotoxic effects against four important tumor cell lines were evaluated. A clear advantage was observed when ATRA-loaded NLC was compared with free ATRA for the MCF-7, MDA-MB-231, HL-60 and Jurkat cell lines.
- For ATRA-resistant cells such as MDA-MB-231 and Jurkat cells, it was suggested that the activity of ATRA-loaded NLC results from the release of butyric acid from TB hydrolysis.
- The effects of treatments in MDA-MB-231 with ATRA-loaded NLC are probably related to some degree of aneuploidy (DNA content different from 2n).
- Flow cytometry assay was employed as a quantitative measure of subdiploid DNA content and phases of the cell cycle. ATRA-loaded NLC showed a significant accumulation in the $G_0/G_1$ phase when compared with free ATRA for all cell lines.
- None of the treatments induced significant cell death, with values of subdiploid DNA content less than 1%. These findings are not unexpected, once ATRA-induced cell cycle arrest in the $G_0/G_1$ phase is usually followed by differentiation and/or apoptosis.
- A remarkable increase in anticancer activity of ATRA–TB-loaded NLC in comparison with free ATRA was obtained against leukemic cells using a formulation with high drug encapsulation.

## References

Papers of special note have been highlighted as:
• of interest
•• of considerable interest

1. Petrie K, Zelent A, Waxman S. Differentiation therapy of acute myeloid leukemia: past, present and future. Curr Opin Hematol 2009;16:84-91

• **An important review to better understand the specific actions of *all-trans* retinoic acid (ATRA) in treatment of acute myeloid leukemia.**

2. Epstein JB, Gorsky M. Topical application of vitamin A to oral leukoplakia: a clinical case series. Cancer 1999;86:921-7
3. Shimizu K, Tamagawa K, Takahashi N, et al. Stability and antitumor effects of all-trans retinoic acid-loaded liposomes contained sterylglucoside mixture. Int J Pharm 2003;258:45-53
4. Tang XH, Gudas LJ. Retinoids, retinoic acid receptors, and cancer. Annu Rev Pathol 2011;6:345-64
5. Adamson PC, Pitot HC, Balis FM, et al. Variability in the oral bioavailability of all-trans-retinoic acid. J Natl Cancer Inst 1993;85:993-6
6. Muindi JR, Frankel SR, Huselton C, et al. Clinical pharmacology of oral all-trans retinoic acid in patients with acute promyelocytic leukemia. Cancer Res 1992;52:2138-42
7. Abdulmajed K, Heard CM. Topical delivery of retinyl ascorbate co-drug. 1. Synthesis, penetration into and permeation across human skin. Int J Pharm 2004;280:113-24
8. Lim SJ, Lee MK, Kim CK. Altered chemical and biological activities of all-trans retinoic acid incorporated in solid lipid nanoparticle powders. J Control Release 2004;100:53-61
9. Chansri N, Kawakami S, Yamashita F, Hashida M. Inhibition of liver metastasis by all-trans retinoic acid incorporated into O/W emulsions in mice. Int J Pharm 2006;321:42-9
10. Chinsriwongkul A, Chareanputtakhun P, Ngawhirunpat T, et al. Nanostructured lipid carriers (NLC) for parenteral delivery of an anticancer drug. AAPS PharmSciTech 2012;13:150-8
11. Radtke M, Souto EB, Müller RH. Nanostructured Lipid Carriers: a novel generation of solid lipid drug carriers. Pharm Tech Eur 2005;17:45-50

•• **A review that helps to understand the concept of nanostructured lipid carriers, their production and possible applications.**

12. Selvamuthukumar S, Velmurugan R. Nanostructured Lipid Carriers: a potential drug carrier for cancer chemotherapy. Lipids Health Dis 2012;11:159

•• **This review shows the different types of nanostructured lipid carriers and discusses how they can be used in cancer chemotherapy.**

13. Varshosaz J, Hassanzadeh F, Sadegh H, Andalib S. Synthesis of octadecylamine-retinoic acid conjugate for enhanced cytotoxic effects of 5-FU using LDL targeted nanostructured lipid carriers. Eur J Med Chem 2012;4:429-38
14. Castro GA, Orefice RL, Vilela JM, et al. Development of a new solid lipid nanoparticle formulation containing retinoic acid for topical treatment of acne. J Microencapsul 2007;24:395-407

• **This paper reports the use of lipophilic amines as an interesting alternative to increase ATRA encapsulation in lipid nanoparticles due to the formation of an ion pairing.**

15. Carneiro G, Silva EL, Pacheco LA, et al. Formation of ion pairing as an alternative to improve encapsulation and anticancer activity of all-trans retinoic acid loaded in solid lipid nanoparticles. Int J Nanomedicine 2012;7:6011-20
16. Kim H, Bae S. Histone deacetylase inhibitors: molecular mechanisms of action and clinical trials as anti-cancer drugs. Am J Transl Res 2011;3:166-79

•• **This review provides important information concerning the molecular mechanisms of action of histone deacetylase inhibitors and their application in cancer therapy.**

17. Su J, Zhang N, Ho PC. Evaluation of the pharmacokinetics of All-Trans-Retinoic Acid (ATRA) in wistar rats after intravenous administration of ATRA loaded into tributyrin submicron emulsion and its cellular activity on Caco-2 and HepG2 cell lines. J Pharm Sci 2008;97:2844-53
18. Kang SN, Hong S, Lee M, Lim S. Dual function of tributyrin emulsion: solubilization and enhancement of anticancer effect of celecoxib. Int J Pharm 2012;428:76-81
19. Castro GA, Coelho AL, Oliveira CA, et al. Formation of ion pairing as an alternative to improve encapsulation and stability and to reduce skin irritation of retinoic acid loaded in solid lipid nanoparticles. Int J Pharm 2009;381:77-83
20. Riccardi C, Nicoletti I. Analysis of apoptosis by propidium iodide staining and flow cytometry. Nat Protoc 2006;1:1458-61
21. Hong TK, Lee-Kim YC. Effects of retinoic acid isomers on apoptosis and enzymatic antioxidant system in human breast cancer cells. Nutr Res Pract 2009;3:77-83
22. Mangiarotti R, Danova M, Alberici R, Pellicciari C. All-trans retinoic acid (ATRA)-induced apoptosis is preceded by G1 arrest in human MCF-7 breast cancer cells. Br J Cancer 1998;77:186-91
23. Li RJ, Ying X, Zhang Y, et al. All-trans retinoic acid stealth liposomes prevent the relapse of breast cancer arising from the cancer stem cells. J Control Release 2011;149:281-91
24. Rishi AK, Gerald TM, Shao ZM, et al. Regulation of the human retinoic acid receptor $\alpha$ gene in the estrogen receptor negative human breast carcinoma cell lines SKBR-3 and MDA-MB-4351. Cancer Res 1996;56:5246-52
25. Chen G, Bradford WD, Seidel CW, Li R. Hsp90 stress potentiates rapid cellular adaptation through induction of aneuploidy. Nature 2012;482(7384):246-50
26. Cappello P, Blaser H, Gorrini C, et al. Role of Nek2 on centrosome duplication and aneuploidy in breast cancer cells. Oncogene 2014;33:2375-84
27. Sartore RC, Campos PB, Trujillo CA, et al. Retinoic acid-treated pluripotent stem cells undergoing neurogenesis present increased aneuploidy and micronuclei formation. PLoS One 2011;6(6):e20667
28. Galagher RE. Retinoic acid resistance in acute promyelocytic leukemia. Leukemia 2002;16:1940-58
29. Yamaguchi T, Maeda Y, Ueda S, et al. Dichotomy of all-trans retinoic acid inducing signals for adult T-cell leukemia. Leukemia 2005;9:1010-17
30. Kurita-Ochiai T, Fukushima K, Ochiai K. Butyric acid-induced apoptosis of murine thymocytes, splenic T cells, and human jurkat T cells. Infection and Imnunity 1997;65: 35-41
31. Noy N. Between death and survival: retinoic acid in regulation of apoptosis. Annu Rev Nutr 2010;30:201-17

•• **A very interesting review that explains the mechanism of action of ATRA in regulation of apoptosis.**

32. Leszczyniecka M, Roberts T, Dent P, et al. Differentiation therapy of human cancer: basic science and clinical applications. Pharmacol Ther 2001;90:105-56

•• **Excellent review on differentiation therapy, giving its concept, molecular basis and several types of differentiation agents, especially those applied to hematological malignancies.**